



# Development of Fault Models for Hybrid Fault Detection and Diagnostics Algorithm

October 1, 2014 — May 5, 2015

Howard Cheung and James E. Braun  
*Purdue University*  
*West Lafayette, Indiana*

NREL Technical Monitor: Stephen Frank

**NREL is a national laboratory of the U.S. Department of Energy  
Office of Energy Efficiency & Renewable Energy  
Operated by the Alliance for Sustainable Energy, LLC**

This report is available at no cost from the National Renewable Energy  
Laboratory (NREL) at [www.nrel.gov/publications](http://www.nrel.gov/publications).

**Subcontract Report**  
NREL/SR-5500-65030  
December 2015

Contract No. DE-AC36-08GO28308



# Development of Fault Models for Hybrid Fault Detection and Diagnostics Algorithm

October 1, 2014 — May 5, 2015

Howard Cheung and James E. Braun  
*Purdue University*  
*West Lafayette, Indiana*

NREL Technical Monitor: Stephen Frank  
Prepared under Subcontract No. XGG-4-42185-01

**NREL is a national laboratory of the U.S. Department of Energy  
Office of Energy Efficiency & Renewable Energy  
Operated by the Alliance for Sustainable Energy, LLC**

This report is available at no cost from the National Renewable Energy  
Laboratory (NREL) at [www.nrel.gov/publications](http://www.nrel.gov/publications).

National Renewable Energy Laboratory  
15013 Denver West Parkway  
Golden, CO 80401  
303-275-3000 • [www.nrel.gov](http://www.nrel.gov)

**Subcontract Report**  
NREL/SR-5500-65030  
December 2015

Contract No. DE-AC36-08GO28308

## NOTICE

This report was prepared as an account of work sponsored by an agency of the United States government. Neither the United States government nor any agency thereof, nor any of their employees, makes any warranty, express or implied, or assumes any legal liability or responsibility for the accuracy, completeness, or usefulness of any information, apparatus, product, or process disclosed, or represents that its use would not infringe privately owned rights. Reference herein to any specific commercial product, process, or service by trade name, trademark, manufacturer, or otherwise does not necessarily constitute or imply its endorsement, recommendation, or favoring by the United States government or any agency thereof. The views and opinions of authors expressed herein do not necessarily state or reflect those of the United States government or any agency thereof.

This report is available at no cost from the National Renewable Energy Laboratory (NREL) at [www.nrel.gov/publications](http://www.nrel.gov/publications).

Available electronically at SciTech Connect <http://www.osti.gov/scitech>

Available for a processing fee to U.S. Department of Energy and its contractors, in paper, from:

U.S. Department of Energy  
Office of Scientific and Technical Information  
P.O. Box 62  
Oak Ridge, TN 37831-0062  
OSTI <http://www.osti.gov>  
Phone: 865.576.8401  
Fax: 865.576.5728  
Email: [reports@osti.gov](mailto:reports@osti.gov)

Available for sale to the public, in paper, from:

U.S. Department of Commerce  
National Technical Information Service  
5301 Shawnee Road  
Alexandria, VA 22312  
NTIS <http://www.ntis.gov>  
Phone: 800.553.6847 or 703.605.6000  
Fax: 703.605.6900  
Email: [orders@ntis.gov](mailto:orders@ntis.gov)

*Cover Photos by Dennis Schroeder: (left to right) NREL 26173, NREL 18302, NREL 19758, NREL 29642, NREL 19795.*

NREL prints on paper that contains recycled content.

## List of Acronyms

AHU	air handling unit
COP	coefficient of performance
DX	direct expansion
FDD	fault detection and diagnostics
GJ	gigajoule
HVAC	heating, ventilating, and air conditioning
kW	kilowatt
MEC	Modified Education Center
N/A	not available
RTU	rooftop unit
SEB	(East) Site Entrance Building
VAV	variable air volume

## Nomenclature

A	DX coil model empirical coefficients (unit varies)
C	empirical coefficients in fault models (unit varies)
BF	bypass factor (dimensionless)
$c_p$	specific heat capacity (J/kg-K)
$\Delta P$	pressure difference (Pa)
EIR	energy input ratio (dimensionless)
F	function (dimensionless)
Freq	rotational speed (Hz)
F	fault level (dimensionless)
H	enthalpy (J/kg)
$\dot{m}$	mass flow rate (kg/s)
$\Omega$	humidity ratio (kg of water/ kg of dry air)
$\dot{Q}$	cooling capacity (W)
$r^2$	coefficient of determination
SHR	sensible heat ratio (dimensionless)
T	temperature (K)
UA	heat transfer conductance (W-K)
V	volumetric air flow rate (m <sup>3</sup> /s)
$\dot{W}$	power consumption (W)

### Subscript

A	air-water mixture
Adp	saturated at coil surface
Amb	outside
Cond	condenser
Cool	cooling
Chiller	chiller
Db	dry-bulb
Duct	air duct
Dx	DX coil model
Ent	DX coil inlet
F	faulted
Fan	fan
Lvg	DX coil outlet
Rat	rated condition
W	water
Wb	wet-bulb

## Acknowledgments

The authors would like to acknowledge Rongpeng Zhang and Tianzhen Hong from Lawrence Berkeley National Laboratory for their discussion related to the input and output structure of the duct fouling model. The authors would also like to acknowledge Joseph Robertson for creating the Ruby scripts to implement the models of no thermostat set point reset on weekends and thermostat bias in OpenStudio for the project.

## Executive Summary

This report describes models of building faults that were created for OpenStudio to support the ongoing development of fault detection and diagnostic (FDD) algorithms at the National Renewable Energy Laboratory. Building faults are operating abnormalities that degrade building performance, which include using more energy than normal operation or failing to maintain building temperatures according to the thermostat set points. Models of building faults in OpenStudio can be used to estimate fault impacts on building performance and to develop and evaluate FDD algorithms.

The aim of the project was to develop fault models for typical heating, ventilating, and air-conditioning (HVAC) equipment in the United States. The fault models in this report are grouped as follows:

- Control fault models, which simulate the impacts of inappropriate thermostat control schemes such as an incorrect thermostat set point in unoccupied hours and manual changes of thermostat set point due to extreme outside temperatures
- Sensor fault models, which focus on the modeling of sensor biases including economizer relative humidity sensor bias, supply air temperature sensor bias, and water circuit temperature sensor bias
- Packaged and split air conditioner fault models, which simulate refrigerant undercharging, condenser fouling, condenser fan motor efficiency degradation, noncondensable entrainment in the refrigerant, and liquid line restriction
- Water-cooled chiller fault models, which simulate refrigerant overcharging, excessive oil, noncondensable entrainment in the refrigerant, and condenser fouling
- Other uncategorized fault models, which include duct fouling, excessive infiltration into the building, and blower and pump motor degradation.

Three modeling techniques were used—empirical modeling, semiempirical modeling, and physical modeling. Empirical models were used mainly to model air conditioner and chiller faults with training data obtained from simulation or testing of equipment. Semiempirical models were used mainly for motor faults and duct faults; other fault models were created based on physical principles. Validation results for these models are discussed in the appendices.

To verify expected behaviors for the various faults, models of two buildings were used with the fault models; annual energy consumption was estimated for various scenarios. The building model with a split air conditioner was tested with the air conditioner fault models only; the other fault models were imposed within a building model that used a water-cooled chiller for space cooling. All that building's gas use was for heating. These building models were taken from previous work, because they provided a convenient starting point for this project and because high-quality weather and calibration data were readily available. However, these models had some limitations. The highly energy-efficient design of the buildings and the big diurnal temperature variations of the climate relative to typical buildings tended to reduce the sensitivity of the models to some of the faults. Also, the nonfaulted thermostat control strategy in these models did not always ensure comfort in the early morning when occupants arrived; hence, the models were not ideal for testing control fault models. Although the magnitude of the fault

impacts in the simulation results is not representative of typical buildings, the results did show that the fault models executed successfully within the OpenStudio/EnergyPlus environment, and that all fault models affected building electricity or gas consumption as expected. The development of these fault models enables future work to determine the sensitivity of energy use to the faults in a variety of typical buildings in a variety of climates.

To conclude, the fault models can change the building performance realistically according to the definition and the mechanism of the faults. These fault models can:

- Simulate changes in building operation with the faults
- Be used to understand how faults affect building operation and energy consumption
- Provide information for FDD algorithm development.

The library of fault models in the form of OpenStudio Measure scripts is available to the public at the NREL/OpenStudio-fault-models website at <https://github.com/NREL/OpenStudio-fault-models>.

# Table of Contents

<b>1</b>	<b>Introduction</b>	<b>1</b>
<b>2</b>	<b>Literature Review</b>	<b>3</b>
<b>3</b>	<b>Fault Description</b>	<b>4</b>
3.1	Control Faults	4
3.1.1	No Overnight Setback	4
3.1.2	Extended Morning or Evening Thermostat Set Points	4
3.1.3	Manual Changes of Thermostat Set Point Due to Extreme Outside Temperatures	4
3.2	Sensor Faults	5
3.2.1	Temperature and Relative Humidity Sensor Biases	5
3.3	Rooftop Unit and Air Conditioner System Faults	5
3.3.1	Undercharged Rooftop Units and Split Air Conditioners	5
3.3.2	Condenser Fouling in Rooftop Units and Split Air Conditioners	5
3.3.3	Liquid Line Restriction in Rooftop Units	5
3.3.4	Noncondensable Entrainment in Refrigerant in Rooftop Units	6
3.3.5	Motor Efficiency Degradation of Condenser Fans	6
3.4	Chiller Faults	6
3.4.1	Overcharged Chiller	6
3.4.2	Excessive Oil in Chiller	6
3.4.3	Condenser Fouling in Chillers	6
3.4.4	Noncondensable Entrainment in Refrigerant in Chillers	7
3.5	Other Uncategorized Faults	7
3.5.1	Duct Fouling	7
3.5.2	Motor Efficiency Degradation in Blowers and Pumps	7
3.5.3	Excessive Infiltration around the Building Envelope	7
<b>4</b>	<b>Fault Model Development</b>	<b>8</b>
4.1	Empirical Models	8
4.2	Semiempirical Models	9
4.3	Physical Models	10
<b>5</b>	<b>Building Models</b>	<b>11</b>
5.1	East Site Entrance Building Model	11
5.2	Modified Education Center Building Model	12
<b>6</b>	<b>Fault Impacts on Building Energy Consumption</b>	<b>16</b>
<b>7</b>	<b>Conclusion</b>	<b>19</b>
	<b>References</b>	<b>20</b>
	<b>Appendix A: Review of Statistical Measures</b>	<b>23</b>
	<b>Appendix B: Control Faults</b>	<b>24</b>
	<b>Appendix C: Sensor Faults</b>	<b>28</b>
	<b>Appendix D: Rooftop Unit and Split Air Conditioner Fault</b>	<b>34</b>
	<b>Appendix E: Chiller Faults</b>	<b>48</b>
	<b>Appendix F: Other Uncategorized Faults</b>	<b>54</b>

# List of Figures

Figure 1. Diagram of the gas furnace and the split air conditioner installation in the SEB.....	11
Figure 2. The natural gas boiler with three heating coils in the AHUs in the MEC .....	13
Figure 3. The chiller and the cooling tower with three cooling coils in the AHUs in the MEC.....	13
Figure 4. The components of each AHU in the MEC.....	14
Figure C-1. Difference in the outdoor air mass flow rate through the economizer damper .....	29
Figure C-2. Difference in gas consumption, AHU air mass flow rate, and building heat loss .....	32
Figure C-3. Zone air temperature of the case with supply air temperature bias .....	33
Figure D-1. Comparison of fault impact ratios of energy input ratio of split air conditioners .....	38
Figure D-2. Changes in the ratios of sensible heat ratio .....	40
Figure D-3. Comparison of fault impact ratios of energy input ratio of RTUs.....	41
Figure D-4. Comparison of fault impact ratios of energy input ratio of split air conditioners .....	41
Figure E-1. Change of estimation deviation of the chiller noncondensable entrainment fault model with the fault level.....	51
Figure E-2. Change of fault impact ratio of power consumption with noncondensable entrainment fault level.....	52
Figure F-1. Fan and duct curves under normal and fouling condition.....	54
Figure F-2. Residual plot of estimated pressure difference ratio across fans .....	56

## List of Tables

Table 1. List of Fault Models.....	2
Table 2. Appendices Describing the Details of the Fault Models.....	8
Table 3. List of Empirical Fault Models.....	9
Table 4. List of Semiempirical Fault Models.....	10
Table 5. List of Physical Fault Models.....	10
Table 6. Baseline Simulation Results of SEB Model with 2012 Weather Data.....	12
Table 7. Baseline Simulation Results of MEC Model with 2012 Weather Data.....	15
Table 8. Changes in SEB Building Energy Consumption Due to Faults in 2012.....	16
Table 9. Changes in MEC Building Energy Consumption in 2012.....	17
Table B-1. Changes in MEC Building Performance with No Setback Fault.....	24
Table B-2. Changes in MEC Building Performance with Extended Morning Set Point for 3 Hours.....	25
Table B-3. Changes in MEC Building Performance with Extended Evening Set Point for 3 Hours.....	26
Table B-4. Changes in MEC Building Performance with Manual Reduction of Cooling Thermostat Set Point.....	27
Table B-5. Changes in MEC Building Performance with Manual Increase of Heating Thermostat Set Point.....	27
Table C-1. Changes in MEC Building Performance with Return Air Relative Humidity Sensor Bias +3%.....	28
Table C-2. Changes in MEC Building Performance with Ambient Air Relative Humidity Sensor Bias -3%.....	29
Table C-3. Changes in MEC Building Performance with Temperature Sensor Bias.....	30
Table C-4. Changes in MEC Building Performance with Temperature Sensor Bias.....	31
Table C-5. Changes in MEC Building Performance with Temperature Sensor Bias.....	31
Table D-1. Environmental Conditions in Training Data of Empirical Models.....	36
Table D-2. System Specification in Training Data of Empirical Models.....	36
Table D-3. Statistics of the Estimation Results of Fault Models for Undercharged RTUs and Split Air Conditioners.....	37
Table D-4. Change in Simulation Result of SEB Model Because of 30% Undercharging.....	38
Table D-5. Change in Simulation Result of SEB Model Because of 30% Undercharging.....	39
Table D-6. Statistics of the Estimation Results of Condenser Fouling Models.....	40
Table D-7. Changes in Simulation Result of SEB Model Because of 50% Condenser Fouling.....	42
Table D-8. Changes in Simulation Result of SEB Model Because of 50% Condenser Fouling.....	42
Table D-9. Statistics of the Accuracy of the Liquid Line Restriction Model for RTUs.....	43
Table D-10. Change in Simulation Result of SEB Model Because of 30% Liquid Line Restriction.....	44
Table D-11. Statistics of the Accuracy of the Liquid Line Restriction Model for RTUs.....	44
Table D-12. Changes in Simulation Result of SEB Model Because of 60% Noncondensable.....	45
Table D-13. Summary of Specifications of Air Conditioners.....	46
Table D-14. Changes in Simulation Result of SEB Model.....	47
Table D-15. Changes in Simulation Result of SEB Model.....	47
Table E-1. Testing Conditions of Training Data of Chiller Fault Models.....	48
Table E-2. Statistics of the Accuracy of Overcharging Model for Chillers.....	49
Table E-3. Changes in MEC Building Performance With Chiller Overcharged at 30%.....	49
Table E-4. Statistics of the Accuracy of Excessive Oil Model for Chillers.....	50
Table E-5. Changes in MEC Building Performance with the Chiller Faulted by Excessive Oil at 70%.....	50
Table E-6. Statistics of the Accuracy of Noncondensable Entrainment Fault Model for Chillers.....	51
Table E-7. Changes in MEC Building Performance with the Chiller Faulted.....	52
Table E-8. Statistics of the Accuracy of Condenser Fouling Model for Chillers.....	53

Table E-9. Changes in MEC Building Performance with the Chiller Faulted by Condenser Fouling at 40%.....	53
Table F-1. Statistics of the Accuracy of Condenser Fouling Model for Chillers.....	56
Table F-2. Changes in MEC Building Performance by Duct Fouling at 10%.....	57
Table F-3. Changes in MEC Building Performance by Blower Motor Efficiency Degradation at 25%.....	57
Table F-4. Changes in MEC Building Performance by Pump Motor Efficiency Degradation at 15% .....	58
Table F-5. Changes in MEC Building Performance by Excessive Infiltration at 30%.....	59

# 1 Introduction

Heating, ventilating, and air-conditioning (HVAC) equipment and control schemes in modern buildings are designed to meet multiple needs such as occupant thermal comfort, ventilation, and energy efficiency to economically support the buildings' activities. Although the buildings may meet these requirements immediately after construction and commissioning, intrinsic or new faults may cause their performance to gradually decline. For instance, condenser fouling in chillers increases energy consumption (Comstock et al. 2001). Refrigerant leakage can also reduce efficiency and diminish comfort (Shen et al. 2011). These issues force the building equipment to work in off-design conditions that compromise energy efficiency and comfort.

Some limited studies have been conducted to understand the prevalence of building faults in the field. Comstock (1999) surveyed repair records from field technicians and found that control box failures were the most common problem in water-cooled centrifugal chillers, followed by refrigerant leakage and condenser fouling. Jacobs et al. (2003) surveyed the prevalence of faults in packaged air conditioners (rooftop units [RTUs]). They found that 63% of economizers in RTUs were malfunctioning and 39% were running with indoor airflows lower than the design requirement or with fan power consumption higher than expected.

Although faults are highly prevalent in the field, conducting thorough, regular, and manual equipment maintenance to detect and fix the faults is difficult and costly. Thus, multiple fault detection and diagnostics (FDD) tools have been developed to automate the process and reduce its cost. Usoro et al. (1985) described a Kalman filter-based algorithm to detect faults in air handling units (AHUs). Other efforts to create methodologies for FDD tools for various types of HVAC equipment in buildings included chillers (Castro 2002; Reddy 2007), variable air volume (VAV) terminals (Wang and Qin 2005; Xiao et al. 2014), RTUs (Breuker and Braun 1998; Kim and Braun 2013), and sensors (Wang et al. 2010; Yang et al. 2013). Some FDD tools have been developed to diagnose faults at the building level (Henze et al. 2015). Katipamula and Brambley (2005a,b) provide more details in a review of FDD tool development for HVAC equipment.

To develop an FDD method that is applicable to multiple HVAC systems in one building, the National Renewable Energy Laboratory (NREL) is conducting an ongoing study to develop machine-learning-based FDD tools that rely on training data that are generated by calibrated building energy models and building fault models. These tools require fault models that can be applied to building energy models, and this report describes the fault models that have been created to support the FDD algorithm development (Table 1).

Some fault models that were used to support the FDD algorithm development are not described in this report because they were developed before the subcontract period began. For instance, the model of no reset of thermostat set point on weekends is not discussed in this report because it was developed by project team members Paulo Cesar Tabares Velasco and Joseph Robertson before the reported project period. A thermostat bias model used to develop the FDD tool was developed by Basarkar et al. (2011); its modeling approach is not described in this report. Three other faults—economizer damper stuck fault, economizer temperature sensor bias, and duct leakage fault—are also not described in this report, because their models are identical to fault models present in EnergyPlus version 8.1.

**Table 1. List of Fault Models**

<b>Types of Faults</b>	<b>Fault Models</b>
<b>Control faults</b>	<ul style="list-style-type: none"><li>• No overnight setback of thermostat set point</li><li>• Extended morning or evening thermostat set points</li><li>• Manual change of thermostat set point due to extreme outside temperature.</li></ul>
<b>Sensor faults</b>	<ul style="list-style-type: none"><li>• Economizer relative humidity sensor bias</li><li>• Bias of temperature sensors on water circuits</li><li>• Supply air temperature sensor bias.</li></ul>
<b>RTU and split air conditioner faults</b>	<ul style="list-style-type: none"><li>• Undercharged air conditioner</li><li>• Condenser fouling</li><li>• Liquid line restriction</li><li>• Noncondensable entrainment in refrigerant flow</li><li>• Condenser fan motor efficiency degradation.</li></ul>
<b>Chiller faults</b>	<ul style="list-style-type: none"><li>• Overcharged chiller</li><li>• Chiller with excessive oil</li><li>• Noncondensable entrainment in refrigerant flow</li><li>• Chiller with condenser fouling.</li></ul>
<b>Other uncategorized faults</b>	<ul style="list-style-type: none"><li>• Duct fouling</li><li>• Blower motor efficiency degradation</li><li>• Pump motor efficiency degradation</li><li>• Excessive infiltration around building envelope.</li></ul>

The remainder of this report is summarized here:

- Section 2: A literature review on building faults and their models
- Section 3: Brief descriptions of the faults
- Section 4: Fault model development
- Sections 5 and 6: Building energy models used to demonstrate the fault models
- Section 7: Conclusions about the findings and contribution of the fault modeling project
- Appendices: Details about individual fault models.

## 2 Literature Review

This literature review provides a basis for the application of available fault models and the creation of new ones to support the development and evaluation of FDD tools that use building energy models.

Some fault models were developed to support FDD tools such as the current project. For instance, Zhou et al. (2009) considered how heat exchanger effectiveness changes with fouling. Zhao et al. (2014) created a chiller model for faulty operation using machine learning as part of their chiller FDD algorithm. Zhao et al. (2012) developed a virtual condenser water flow sensor to estimate the change of coil heat transfer conductance under various faulted conditions. These fault models require training data from experimental testing under faulty conditions for each new piece of equipment. Although they might be economically viable for FDD tools on a single equipment model, the number of faults that can occur in a building is so large that creating a new fault model for every new piece of equipment is impossible. This approach is thus unsuitable for the current FDD algorithm project.

Some projects simulated impacts of faults to quantify how equipment performance changes with the fault levels. Other projects created void fraction models (Rice 1987) to accurately estimate the amount of refrigerant inside heat exchangers and still others created a tuning equation (Rossi 1995; Shen 2006; Cheung and Braun 2013) to accurately estimate the refrigerant amount inside a vapor compression system. These projects also quantified the impacts of other faults by using physics-based principles such as reducing airflow to model air-side fouling and by adding a refrigerant flow bypass around the compressor to model valve leakage. However, these methods are not suitable for the current project because they require information—such as heat exchanger volume and the size of compressor—that cannot be obtained from building energy modelers.

Building simulation programs were also used to develop fault models to study the impacts of building faults. Empirical models of faults that directly affect refrigerant flow in a split system such as charge leakage and noncondensable entrainment in refrigerant were modeled by Cho et al. (2014), and the models were used by Domanski et al. (2014) to study their impacts for a residential building. Basarkar et al. (2011) modeled stuck economizer damper and temperature sensor offset faults in the building simulation program EnergyPlus. These fault models, together with fault models of economizer sensor bias, were programmed into the source code of EnergyPlus and were released in its version 8.1. These fault models are suitable for the current development of FDD algorithms, but more models are needed to increase the types of faults against which the developing FDD algorithms can be tested.

## 3 Fault Description

This section describes the causes and definitions of faults in this report. It also explains the definition of fault level that is used to define the fault numerically in the fault models. They include control faults, sensor faults, RTU and split air conditioner faults, chiller faults, and other uncategorized faults.

### 3.1 Control Faults

Control faults are faults in the control scheme of the operation of the building equipment. Three control faults are studied in this report:

- No overnight setback
- Extended morning and evening thermostat set points
- Manual changes of thermostat set point due to extreme outside temperatures.

This section gives a simple description of the control faults; other details such as the fault level definitions are given in Appendix B.

#### 3.1.1 *No Overnight Setback*

This fault occurs when building managers do not establish a thermostat set point to reduce energy consumption during unoccupied hours. Set points can be lowered in the heating season and increased in the cooling season during unoccupied hours. If the set point remains the same in occupied and unoccupied hours, the building consumes more energy than necessary.

#### 3.1.2 *Extended Morning or Evening Thermostat Set Points*

This fault occurs when building managers extend thermostat set points of the optimized schedule incorrectly into unoccupied hours because they misunderstand the occupant schedule or the need to preheat or precool the building before occupancy. Similar to the no overnight setback fault, the building with extended schedules consumes more energy for space conditioning than necessary. However, if the building thermostat set point schedule is not optimized for thermal comfort and an extension of the thermostat set point to the early morning improves occupants' thermal comfort by precooling or preheating the building, the extension should not be considered a building fault. The fault level is the number of hours the thermostat set point in occupied hours is extended toward the evening or the morning.

#### 3.1.3 *Manual Changes of Thermostat Set Point Due to Extreme Outside Temperatures*

This fault occurs when occupants change the thermostat set point regardless of the building manager's directives. On days with extreme outside temperatures, occupants may feel too cold or too hot after entering a conditioned zone and demand more heating or cooling than expected. They may change the thermostat set point without instructions and increase the energy consumption of the HVAC equipment. This increase is considered unnecessary and is modeled as a fault. In the heating season, the fault is defined by the highest outside temperature occupants will change the thermostats to and the subsequent increase of the heating set point. In the cooling season, the fault is defined by the lowest outside temperature occupants change the thermostats to and the subsequent reduction of the cooling set point.

## **3.2 Sensor Faults**

These faults occur when sensors operate incorrectly. This report studies only the sensor faults in temperature and relative humidity sensors as a result of sensor biases.

### **3.2.1 Temperature and Relative Humidity Sensor Biases**

This fault occurs when sensors drift and are not regularly calibrated. Sensor readings drift from their calibration with age; therefore, equipment control algorithms produce readings that vary from true operating conditions. This can lead to more energy use, temperatures that vary significantly from the thermostat set point, insufficient ventilation, etc. The fault level is defined by the difference between the sensor readings and the true properties the sensors should read. Appendix C provides a detailed explanation of how biases of sensors at various locations in the buildings affect the building operation.

## **3.3 Rooftop Unit and Air Conditioner System Faults**

This subsection describes the faults of the refrigerant circuits and the condenser fan in RTUs and split air conditioners. The faults include an incorrect amount of refrigerant in the air conditioner, condenser fouling, liquid line restriction, and noncondensable entrainment in the refrigerant flow. This subsection gives a general description of the faults; additional details about the faults are provided in Appendix D.

### **3.3.1 Undercharged Rooftop Units and Split Air Conditioners**

This fault occurs when refrigerant leaks from the refrigerant circuit in air conditioners. Without sufficient refrigerant running in the system, the average refrigerant density, the evaporating temperature, and the refrigerant mass flow rate from the compressor all drop. These drops reduce the total and sensible cooling capacity of the air conditioner, lengthen its operating time, and increase its energy consumption. The fault level is defined by the percentage reduction of the mass of refrigerant in the faulted air conditioner from the manufacturer's recommendation.

### **3.3.2 Condenser Fouling in Rooftop Units and Split Air Conditioners**

This fault occurs when litter or dirt accumulates between the fins of an air conditioner condenser located in the outdoor environment. The blockage reduces the airflow across the condenser and increases the condensing temperature in the refrigerant circuit. This increases the pressure difference across the compressor and by extension its power consumption. The fault level is defined as the percentage reduction of condenser airflow.

### **3.3.3 Liquid Line Restriction in Rooftop Units**

This fault occurs when dirt accumulates within the refrigerant filter located between the condenser and the expansion valve in the refrigerant circuit of an RTU. The accumulation increases the flow resistance of the refrigerant circuit and the pressure difference across the compressor. It also reduces the evaporating temperature and leads to lower cooling capacity, efficiency, and sensible heat ratio. The fault level is defined as the percentage difference between the pressure difference between the condenser outlet and evaporator inlet in the restricted case and the pressure difference across the same location in the nonfaulted case.

### **3.3.4 Noncondensable Entrainment in Refrigerant in Rooftop Units**

This fault occurs when the refrigerant unit is not evacuated prior to charging the air conditioner with refrigerant, which causes the air conditioner to run with a mixture of air and refrigerant. Because it is noncondensable, the air inside the refrigerant circuit is trapped in the high-pressure vapor downstream of the compressor, and the pressure difference across the compressor and the compressor power consumption exceeds the normal level. The fault level is defined as the ratio of the mass of air in the air conditioner to the mass of air the refrigerant circuit can hold when the air fills the volume inside the circuit at standard atmospheric pressure.

### **3.3.5 Motor Efficiency Degradation of Condenser Fans**

Motor efficiency degrades when a motor suffers from a bearing or a stator winding fault. These faults will cause the motor to draw higher current from the electricity supply without changing the fluid flow. In other words, they reduce the motor efficiency to convert electricity into mechanical energy without affecting the volumetric flow rate of the fan or pump driven by the motor. The fault level is defined as the percentage reduction of motor efficiency.

## **3.4 Chiller Faults**

This subsection describes chiller faults of the refrigerant system inside the chiller. They include refrigerant overcharging, excessive oil, condenser fouling, and noncondensable entrainment in refrigerant flow. This subsection gives a general description of the faults; additional details about the faults are provided in Appendix E.

### **3.4.1 Overcharged Chiller**

This fault occurs when too much refrigerant is added to a chiller during installation or maintenance. The excess refrigerant resides in the condenser and increases the condensing pressure and pressure difference across the compressor. This increases the power consumption of the chiller. The fault level is defined as the percentage difference between the amount of refrigerant in the refrigerant circuit and the amount of refrigerant recommended by the manufacturer.

### **3.4.2 Excessive Oil in Chiller**

This fault occurs when too much lubricating oil is added to a chiller during installation or maintenance. The excessive oil absorbs some refrigerant from the refrigerant circuit and reduces the amount of effective refrigerant running in the chiller. The chiller's performance is affected in a manner similar to undercharging of RTUs and split air conditioners. The fault level is defined as the percentage difference between the mass of oil in the chiller and the mass of oil recommended by the manufacturer.

### **3.4.3 Condenser Fouling in Chillers**

Condensers are fouled in chillers when dirt accumulates at the condenser water flow path in the condenser from the water supply. Although the medium differs from the condenser of RTUs and split air conditioners, the faults affect the chiller refrigerant circuit in the same way they affect the refrigerant circuits of air conditioners. The fault level is defined as the percentage of water flow paths blocked by condenser fouling.

#### **3.4.4 Noncondensable Entrainment in Refrigerant in Chillers**

This fault occurs in a similar way as the fault of noncondensable entrainment in refrigerant in RTUs. If a chiller is not evacuated completely before charging refrigerant into its refrigerant circuit, the air flows with refrigerant in the refrigerant circuit and undermines the chiller's performance the same way as the noncondensable entrainment fault described in Section 3.3.4.

### **3.5 Other Uncategorized Faults**

This subsection describes faults that cannot be categorized into control faults, sensor faults, RTU and split air conditioner faults, or chiller faults. They are duct fouling, degradation of the efficiency of motors in blowers and pumps, and excessive infiltration around building envelope.

#### **3.5.1 Duct Fouling**

Ducts are fouled when dust accumulates between the fins of indoor heat exchangers or at the filters and increases the flow resistance of the air duct. This may increase the pressure difference, reduce the airflow of the blower, or both depending on the type of blower installed in the duct. Because flow resistance is not defined directly in EnergyPlus, the fault level is defined as the percentage increase of pressure difference across the fan due to duct fouling with reference to its operation at the rated speed.

#### **3.5.2 Motor Efficiency Degradation in Blowers and Pumps**

This fault is caused by the degradation of the motor in blowers and pumps following the same mechanism as the motor efficiency degradation of condenser fan motors described in Section 3.4. It is the same as the condenser fan motor efficiency degradation fault: this increases the motor power consumption without affecting the airflow or water flow across the blowers and the pumps.

#### **3.5.3 Excessive Infiltration around the Building Envelope**

This fault is triggered when windows or doors are left open, which increases the air infiltration into the building. Its fault level is defined as the percentage increase of infiltration airflow relative to its nonfaulted operation.

## 4 Fault Model Development

Because the NREL FDD algorithm will be used with the OpenStudio platform, which uses EnergyPlus as its building simulation engine, the fault models were configured for use with OpenStudio and were written in Ruby scripts. The OpenStudio platform reads the fault models in the Ruby scripts and imposes the fault models within the OpenStudio building model. Mathematical forms of the models are needed to write the fault models in Ruby scripts. The methods to develop the mathematical models can be grouped into three main categories: empirical, semiempirical, and physical models.

This section gives a simple and qualitative description of the modeling approaches of the faults discussed in this report, and Table 2 shows the appendices that describe the detailed mathematical forms of the models and their validation results.

**Table 2. Appendices Describing the Details of the Fault Models**

Appendix	Types of Faults
Appendix B	Control faults
Appendix C	Sensor faults
Appendix D	RTU and split air conditioner faults
Appendix E	Chiller faults
Appendix F	Other uncategorized faults

Appendix A reviews the definition of the statistical measures used to explain the validation results in the other appendices.

### 4.1 Empirical Models

Empirical models are used to model fault impacts on building components that are modeled empirically in EnergyPlus. For instance, empirical fault models are designed for the RTUs to simulate the impacts on compressor and condenser fan power consumption and evaporator cooling capacity, because these features are modeled by the empirical DOE-2 direct expansion (DX) coil model (Brandemuehl et al. 1993) in EnergyPlus. Because the DX coil model is empirical, the effects of faults such as condenser airflow reduction cannot be separated from the DX coil model. Hence the fault effects can be modeled only by adding empirical maps to the EnergyPlus component model.

The empirical nature of these fault models implies that additional training data are needed to estimate their coefficients. The training data usually come from results of previous tests or simulations of fault performance for different HVAC equipment. Regression is used to estimate the empirical coefficients from the training data, and the range of the training data limits the applicability of the resultant map.

Table 3 presents the list of fault models constructed in this way.

**Table 3. List of Empirical Fault Models**

<b>Fault Model</b>	<b>Applicable EnergyPlus Models</b>	<b>Variable(s) Adjusted by the Fault Model</b>
<b>Undercharging RTU</b>	Coil:Cooling:DX:SingleSpeed	Cooling capacity
<b>Undercharging split air conditioners</b>		Power consumption of compressor and condenser fan
<b>Condenser fouling in RTU</b>		Sensible heat ratio
<b>Condenser fouling in split air conditioners</b>		
<b>Condenser fan motor degradation in RTU</b>		
<b>Condenser fan motor degradation in split air conditioners</b>		
<b>Liquid line restriction in RTU</b>		
<b>Noncondensable entrainment in RTU</b>		
<b>Overcharging water-cooled chillers</b>	Chiller:Electric:EIR	Power consumption
<b>Excessive oil in water-cooled chillers</b>		
<b>Condenser fouling in water-cooled chillers</b>		
<b>Noncondensable entrainment in water-cooled chillers</b>		

Appendices D and E include the details of the fault modeling approaches and validation results.

## 4.2 Semiempirical Models

Semiempirical models of fault impacts are used to model faults with EnergyPlus component models that are simplified and when fault impacts can be considered through simple modification with physical principles. For instance, some EnergyPlus fan models do not have fan curves. However, a simple normalized fan curve that is added to the original simple fan model can be used to consider the fault impacts on fan performance. In this case, the normalized fan curve is empirical, but the response of the fan curve to the fault effect is modeled by physical principles; the resultant fault models are considered to be semiempirical.

The semiempirical fault models are listed in Table 4.

Appendix F provides a detailed explanation of the semiempirical modeling approach.

**Table 4. List of Semiempirical Fault Models**

<b>Fault Model</b>	<b>Applicable EnergyPlus Models</b>	<b>Variable(s) Adjusted by the Fault Model</b>
<b>Duct fouling</b>	Fan:ConstantVolume Fan:VariableVolume Fan:OnOff	Pressure difference Airflow rate
<b>Blower motor efficiency degradation</b>	Fan:ConstantVolume Fan:VariableVolume Fan:OnOff	Fan efficiency
<b>Pump motor efficiency degradation</b>	Pump:ConstantSpeed Pump:VariableSpeed	Motor efficiency

### 4.3 Physical Models

Physical models are used to model faults when fault levels are related to the inputs of EnergyPlus component models directly. For instance, the supply air temperature sensor bias is modeled by changing the supply air temperature set point with the fault level directly. The fault models of this type are listed in Table 5.

**Table 5. List of Physical Fault Models**

<b>Fault Model</b>	<b>Applicable EnergyPlus Models</b>	<b>Variable(s) Adjusted by the Fault Model</b>
<b>No overnight setback</b>	Multiple schedule objects	Schedule value
<b>Extended morning or evening thermostat set points</b>		
<b>Manual change of thermostat set point due to extreme outside temperature</b>		
<b>Bias of temperature sensors on water circuits</b>		
<b>Supply air temperature sensor bias</b>		
<b>Economizer relative humidity sensor bias</b>	Controller:OutdoorAir	Outdoor air mass flow rate
<b>Excessive infiltration around building envelope</b>	ZoneInfiltration:DesignFlowRate	Design flow rate

Appendices B and C describe the detailed modeling approaches and verification results of the fault models.

## 5 Building Models

This section describes the building models that were used to test the fault models in this report. The two buildings modeled are located at the NREL South Mountain Table campus in Golden, Colorado. Because the project team does not have access to OpenStudio models of actual buildings that use economizers and water-cooled chillers simultaneously, these pieces of equipment are added to the models of the buildings on the NREL campus so all fault models described in this report can be tested without using models of buildings outside the campus.

These building models from previous work were used because they provided a convenient starting point for this project. However, they were not ideal to test fault models, because (1) the buildings were originally designed to be highly energy efficient, and (2) the diurnal temperature variations in the Golden, Colorado, climate are bigger than in other climates. These factors may reduce the sensitivity of the building models to some faults. Their thermostat control strategy also did not guarantee thermal comfort at times and were not ideal for testing control fault models. For these reasons the results are not representative of how various faults affect building operation in general; however, they are sufficient to determine if the fault model can provide results for the development of the FDD algorithm.

### 5.1 East Site Entrance Building Model

The East Site Entrance Building (SEB) is modeled as an 82-m<sup>2</sup> building with one thermal zone and one plenum zone, a 17-kilowatt (kW) split air conditioner for cooling, and an 8.3-kW (28,000-kBtu/h) gas furnace for heating. The model of the split air conditioner is identical to the model of RTUs, and it can be used to test the fault models of RTUs and split air conditioners. A single-speed blower supplies the conditioned air. Occupants use the building continuously, and it uses a constant cooling thermostat set point of 23.9°C and a constant heating thermostat set point of 18.9°C. The building model was calibrated using utility data in 2013. An illustration of the gas furnace and split system in the building is shown in Figure 1.

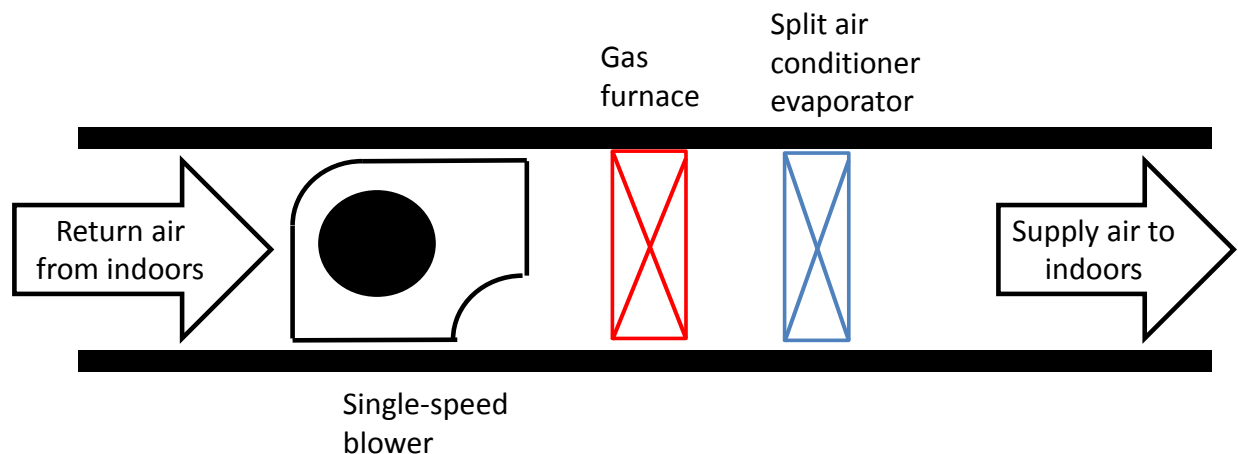


**Figure 1. Diagram of the gas furnace and the split air conditioner installation in the SEB**

In this report, the SEB’s energy consumption in 2012 was used as the nonfaulted operation reference, and the energy consumption was estimated using measured weather data from the NREL campus in Golden, Colorado, for 2012. Table 6 shows the baseline results simulated by EnergyPlus version 8.2. The numbers in parentheses are percentages of the total energy (electrical or gas) associated with a particular end use.

**Table 6. Baseline Simulation Results of SEB Model with 2012 Weather Data**

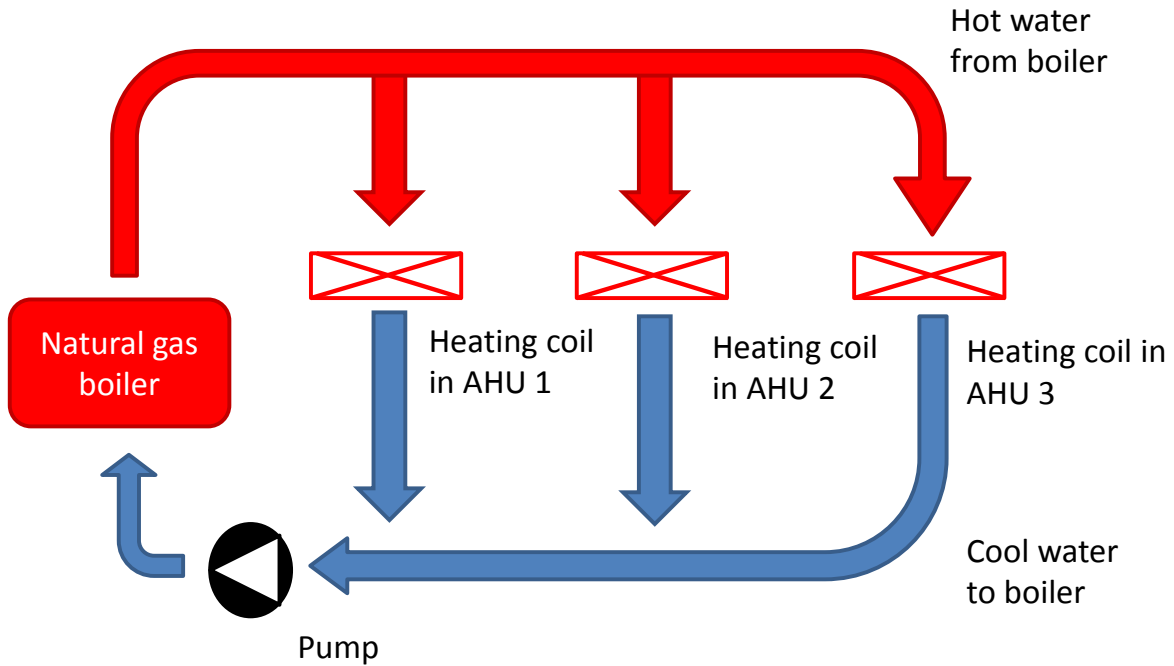
	<b>Electricity Consumption (gigajoules [GJ])</b>	<b>Gas Consumption (GJ)</b>
<b>Compressor and condenser fan of the split system</b>	6.95 (7.8%)	0.00
<b>Blower in the indoor air ducts</b>	14.38 (16.2%)	0.00
<b>Interior equipment and lighting in the building</b>	64.3 (72.4%)	0.00
<b>Gas furnace</b>	0.00	50.63 (100%)
<b>Service water</b>	3.27 (3.7%)	0.00
<b>Overall</b>	88.85	50.63

Table 6 shows that the building used most of its electricity for interior equipment and lighting and only 24% of its electricity for space conditioning.

## 5.2 Modified Education Center Building Model

The original Education Center model contained three thermal zones and one plenum zone with a total floor area of 740 m<sup>2</sup>. It had an air-cooled chiller with a rated cooling capacity of 188 kW and a boiler with a rated heating capacity of 162 kW to condition the space with three AHUs.

However, this model did not have a water-cooled chiller model and an economizer model to test the fault models related to those components. To test these fault models, the air-cooled chiller model was replaced with a water-cooled chiller model with the same rated cooling capacity to produce a Modified Education Center (MEC) building model. A cooling tower was also added, and the parameters of the new models were either calculated by the auto-sizing algorithm in EnergyPlus version 8.2 or came from the default parameters in OpenStudio version 1.6.0. The auto-sized parameters of the cooling tower from EnergyPlus were not sufficient to maintain a cooling tower water outlet temperature at 29.4°C. Therefore, the cooling tower size and flows were increased to meet this requirement. Three economizers were also added to the three AHUs such that they would run at minimum outdoor airflow when the outdoor air enthalpy became higher than that of the return air. The indoor blowers were also configured to run with variable-speed fans with a supply air temperature 12.8°C in cooling season and a supply air temperature 35°C in heating season. The equipment is illustrated in Figure 2 through Figure 4.



**Figure 2. The natural gas boiler with three heating coils in the AHUs in the MEC**

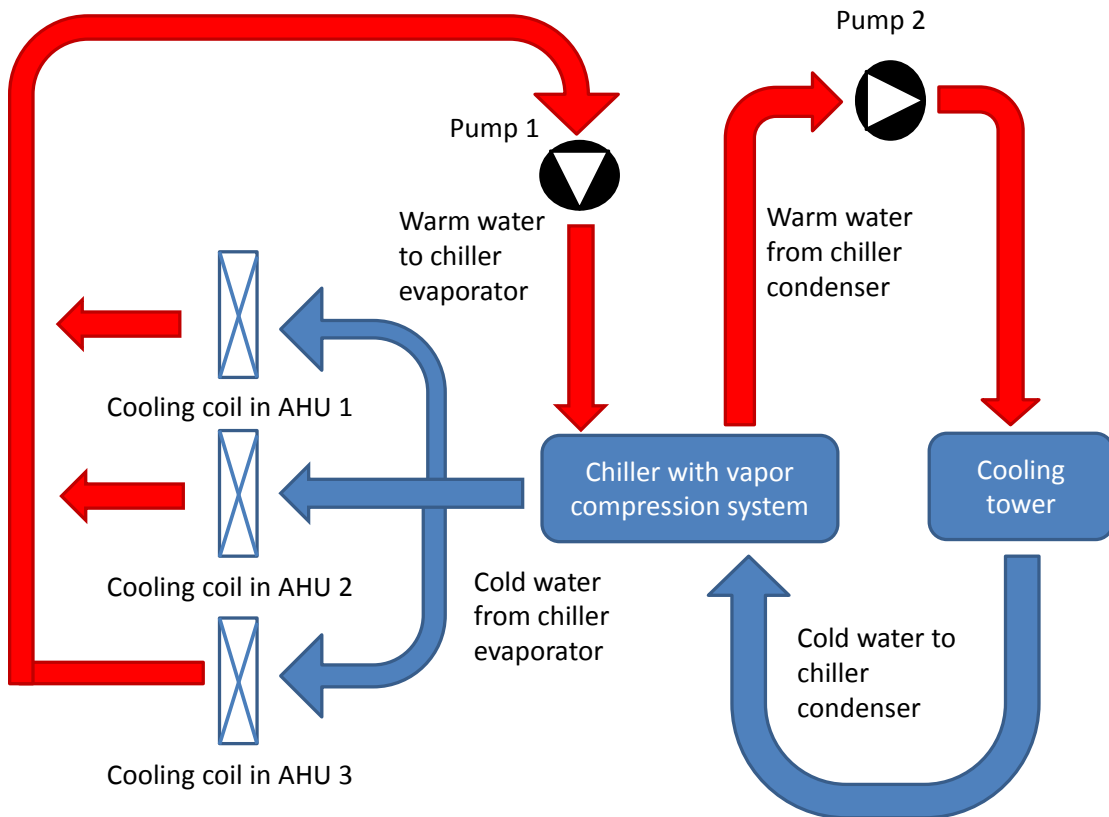


**Figure 3. The chiller and the cooling tower with three cooling coils in the AHUs in the MEC**

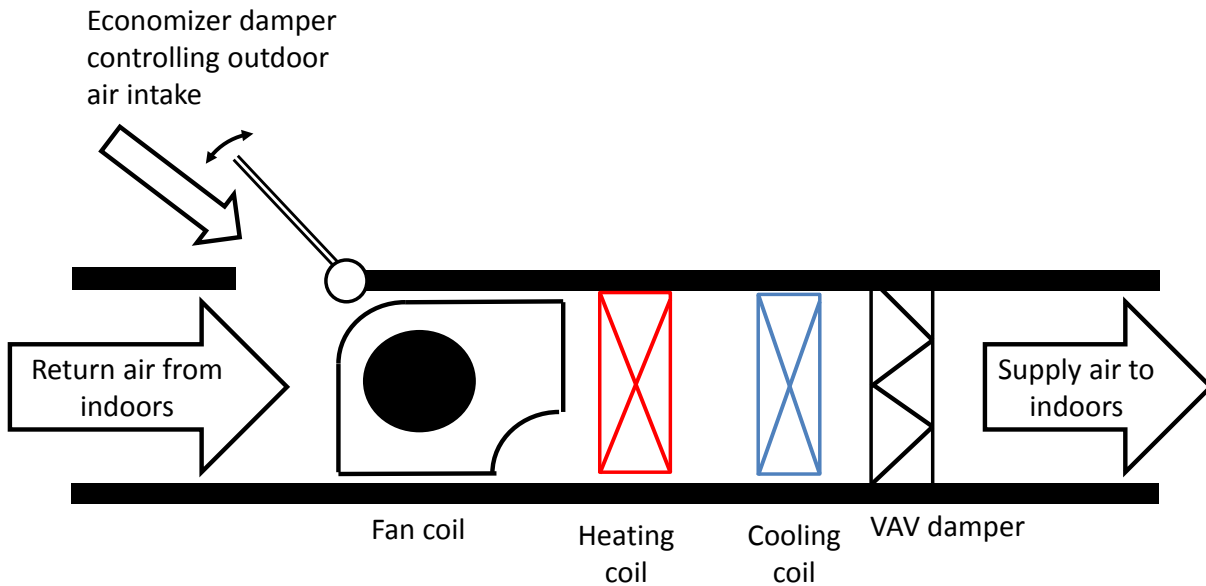


**Figure 4. The components of each AHU in the MEC**

In the model, the Education Center is open on weekdays from 7 a.m. to 6 p.m. and has different thermostat set points between its open and closed hours. During occupied hours, the cooling set point is maintained at 22.2°C and the heating set point is maintained at 20°C. In unoccupied hours, the cooling set point is raised to 26.7°C and the heating set point is reduced to 18.3°C.

Although the thermostat control strategy in the MEC model depends on the occupancy schedule with preheating and precooling and is more suitable to test control fault models than the SEB model, its thermostat control strategy does not ensure thermal comfort on some working days in the beginning of its occupied hours. Because the model is faulty according to occupants' thermal comfort reports on these days before the use of any fault models, studying the impacts of some control fault models using this particular model may cause problems. Nevertheless, the thermostat control strategy was not modified to minimize the changes made to a calibrated building model.

The modified model was simulated with 2012 weather data in Golden, Colorado, for baseline energy consumption values at nonfaulted condition. The baseline simulation results are shown in Table 7.

Table 7 shows that the estimated proportion of electricity used for space conditioning in the MEC is much higher than that of the SEB in Table 6, because the MEC is a larger and different type of building than the SEB.

**Table 7. Baseline Simulation Results of MEC Model with 2012 Weather Data**

	<b>Electricity Consumption (GJ)</b>	<b>Gas Consumption (GJ)</b>
<b>Chiller and cooling tower</b>	379.08 (75.4%)	0.00
<b>Blower in the indoor air ducts</b>	13.39 (2.7%)	0.00
<b>Interior equipment and lighting in the building</b>	76.62 (15.2%)	0.00
<b>Gas furnace</b>	0.00	783.54 (100%)
<b>Pumps for water flow in the chiller, cooling tower, and boiler</b>	24.72 (4.9%)	0.00
<b>Service water heating and pumping</b>	9.16 (1.8%)	0.00
<b>Overall</b>	502.97	783.54

## 6 Fault Impacts on Building Energy Consumption

To assess how faults change building energy consumption, various fault models were imposed within the building models discussed in Section 5 with the same weather data. Although the results are not representative of fault impacts for typical buildings, they are sufficient to verify the fault models behave as expected and can provide training data for developing the FDD algorithm.

RTU and split air conditioner fault models and the control fault model with manual thermostat changes were imposed in the SEB model. Comparisons between annual energy consumption of the faulted and nonfaulted building are tabulated in Table 8.

**Table 8. Changes in SEB Building Energy Consumption Due to Faults in 2012**

<b>Fault Model and Level</b>	<b>Changes in Total Electricity Consumption from Nonfaulted Case (%)</b>	<b>Changes in Total Gas Consumption from Nonfaulted Case (%)</b>
<b>RTU undercharged at 30%</b>	+0.7	+0.0
<b>RTU with condenser fouling at 50%</b>	+1.4	+0.0
<b>RTU with condenser fan motor efficiency degradation at 30%</b>	+0.3	+0.0
<b>RTU with liquid line restriction at 30%</b>	+1.3	+0.0
<b>RTU with noncondensable entrainment at 60%</b>	+0.7	+0.0
<b>Split air conditioners undercharged at 30%</b>	+1.0	+0.0
<b>Split air conditioners with condenser fouling at 50%</b>	+1.1	+0.0
<b>Split air conditioners with condenser fan motor efficiency degradation at 30%</b>	+0.2	+0.0
<b>4K reduction of cooling thermostat set point when outside temperature is higher than 30°C</b>	+0.7	+0.0
<b>4K increase of heating thermostat set point when outside temperature is lower than 5°C</b>	+0.0	+31.3

Table 8 shows that the building's gas consumption remains unchanged for cases with air conditioner faults only. Table 8 also shows that the impacts of the air conditioner faults on total building electricity consumption of the SEB are insignificant, with a maximum change of 1.4%. This is because the compressor and condenser fan, which are directly affected by the faults, use only 7.8% of building electricity (Table 6). If the changes in electricity consumption by the fault are compared to the compressor and condenser fan power consumption, the maximum change is 18.3%. Appendix B includes further explanation of the simulation results.

Table 8 also shows the results of two control faults: the manual changes of heating and cooling thermostat set points as a result of extreme temperature. Similar to the air conditioner faults, the change of cooling set point at high outside temperature increases the electricity for cooling only

and thus the total building electricity use only. The change of the heating thermostat set point affects the heating operation of the building only. Because the building is heated by gas only, the fault increases the total building gas consumption only.

Other fault models were imposed within the MEC model. If a fault model was applicable to more than one component, fault models were imposed within all of them. For instance, when imposing an economizer sensor bias fault model, the fault model was imposed for all economizers in the MEC model at the same fault level. The fault impacts on total building annual energy consumption are tabulated in Table 9.

**Table 9. Changes in MEC Building Energy Consumption in 2012**

<b>Fault Model and Levels</b>	<b>Changes in Total Electricity Consumption from Nonfaulted Case (%)</b>	<b>Changes in Total Gas Consumption from Nonfaulted Case (%)</b>
<b>No overnight setback</b>	+0.1	+1.6
<b>3-hour extension of thermostat set point to the evening</b>	+0.0	+0.1
<b>Chiller water temperature outlet sensor bias at +3K</b>	+0.5	+0.0
<b>Air supply temperature sensor bias at +2K</b>	+11.2	-7.3
<b>Economizer return air relative humidity sensor at +3%</b>	+11.5	+0.9
<b>Economizer ambient air relative humidity sensor at -3%</b>	+12.2	+0.8
<b>Chiller overcharged at 30%</b>	+1.1	+0.0
<b>Chiller with excess oil at 70%</b>	+3.7	+0.0
<b>Chiller with noncondensable entrainment in refrigerant at 5%</b>	+8.7	+0.0
<b>Chiller with condenser fouling at 40%</b>	+2.3	+0.0
<b>Duct fouling at 10%</b>	+0.4	-0.1
<b>Blower motor efficiency degradation at 25%</b>	+1.2	-0.4
<b>Pump motor efficiency degradation at 15%</b>	+1.1	-0.3
<b>Excessive infiltration at 30%</b>	+0.7	+13.3

Table 9 shows that all faults led to an increase in energy consumption of the building; the air supply temperature sensor bias and economizer relative humidity sensor bias faults were the most significant with respect to building electricity consumption. Air supply temperature control is critical to a variable-speed fan system, because it limits the heating and cooling capacity of the AHUs. The relative humidity sensor bias faults are also important because incorrect damper operation may negate the energy savings gained by economizer damper control during cooling operation.

Regarding building gas consumption, Table 9 shows that increased infiltration of cold air in winter was a significant fault that induced a gas consumption increase of 13.3%. As infiltration to the building increased, the high temperature difference between the indoors and outdoors during the winter significantly increased the heating load and gas consumption.

## 7 Conclusion

This report describes fault models that were developed to support NREL in the development of an FDD algorithm for buildings that rely on OpenStudio and EnergyPlus models. The fault models were written in Ruby scripts so they could be implemented within the OpenStudio platform. Models for control faults, sensor faults, faults in refrigerant circuits of air conditioners and chillers, and other faults were developed. The faults were modeled by three methods: empirical, semiempirical, and physical modeling. To verify expected fault behaviors, the fault models were imposed within two building models from previous work. However, these models were not as sensitive to faults as typical buildings because: the buildings were designed to be highly energy efficient, they were simulated in a climate with a bigger diurnal temperature variation than typical climates, and their thermostat control strategy did not ensure thermal comfort. Although the buildings are not typical and the magnitude of the simulation results do not show how the performance of typical buildings is affected by faults, the results did show that the fault models executed successfully within the OpenStudio/EnergyPlus environment, and that the behavior and energy consumption trends associated with each fault model are correct.

The fault models will be used to support the NREL FDD algorithm development by creating training data and test cases to construct and verify the algorithm. Other recommended future work includes applying the fault models to building models representing typical buildings in a variety of climates to characterize fault impacts more broadly. The library of fault models programmed as OpenStudio Measure scripts is now available to the public at the NREL/OpenStudio-fault-models website at <https://github.com/NREL/OpenStudio-fault-models>.

## References

- Basarkar, M., Pang, X., Wang, L., Haves, P., and Hong, T. 2011. "Modeling and Simulation of HVAC Faults in EnergyPlus." *Building Simulation 2011*, Sydney, Australia.
- Bell, I.H., Groll, E.A., and König, H. 2011. "Experimental Analysis of the Effects of Particulate Fouling on Heat Exchanger and Air-Side Pressure Drop for a Hybrid Dry Cooler." *Heat Transfer Engineering*, 32(3):264–71.
- Ben Khader Bouzid, M., and Champenois, G. 2013. "New Expressions of Symmetrical Components of the Induction Motor under Stator Faults." *IEEE Transactions on Industrial Electronics*, 60(9):4093–4102.
- Brandemuehl, M.J., Gabel, S., and Andresen, I. 1993. *HVAC Toolkit: A Toolkit for Secondary HVAC System Energy Calculations*. Atlanta, GA: American Society of Heating, Refrigerating and Air-Conditioning Engineers.
- Breuker, M.S., and Braun, J. E. 1998. "Evaluating the Performance of a Fault Detection and Diagnostic System for Vapor Compression Equipment." *HVAC&R Research*, 4(4):401–25.
- Castro, N.S. 2002. "Performance Evaluation of a Reciprocating Chiller Using Experimental Data and Model Predictions for Fault Detection and Diagnosis." *ASHRAE Transactions*, 108(1):889–903.
- Cheung, H., and Braun, J. E. 2013. "Simulation of Fault Impacts for Vapor Compression Systems by Inverse Modeling. Part II: System Modeling and Validation." *HVAC&R Research*, 19(7):907–21.
- Cho, J.M., Heo, J., Payne, W.V., and Domanski, P.A. 2014. "Normalized Performance Parameters for a Residential Heat Pump in the Cooling Mode With Single Faults Imposed." *Applied Thermal Engineering*, 67:1–15.
- Comstock, M.C. 1999. *Development of Analysis for the Evaluation of Fault Detection and Diagnostics in Chillers*. Master Thesis. West Lafayette, IN: Purdue University.
- Comstock, M.C., Braun, J.E., and Groll, E.A. 2001. "The Sensitivity of Chiller Performance to Common Faults." *HVAC&R Research*, 7(3):263–79.
- da Silva, A.M. 2006. *Induction Motor Fault Diagnostics and Monitoring Methods*. Master Thesis. Milwaukee, WI: Marquette University.
- Domanski, P.A., Henderson, H.I., and Payne, W.V. 2014. "Sensitivity Analysis of Installation Faults on Heat Pump Performance." *NIST Technical Note 1848*. Gaithersburg, MD: National Institute of Standards and Technology.
- Henze, G.P., Pavlak, G.S., Florita, A.R., Dodier, R.H., and Hirsch, A.I. 2015. "An Energy Signal Tool for Decision Support in Building Energy Systems." *Applied Energy*, 138:51–70.

- Jacobs, P., Smith, V., Higgins, C., and Brost, M. 2003. "Small Commercial Rooftops: Field Problems, Solutions, and the Role of Manufacturers." *Proceedings of the 11th National Conference on Building Commissioning*, 20, p. 22.
- Katipamula, S., and Brambley, M.R. 2005a. "Methods for Fault Detection, Diagnostics, and Prognostics for Building Systems—A Review, Part I." *HVAC&R Research*, 11(1):3–25.
- Katipamula, S.; Brambley, M.R. 2005b. "Methods for Fault Detection, Diagnostics, and Prognostics for Building Systems—A Review, Part II." *HVAC&R Research* (12:2); pp 169-87.
- Kim, M., Payne, W.V., Domanski, P.A., Yoon, S.H., and Hermes, C.J.L. 2009. "Performance of a Residential Heat Pump Operating in the Cooling Mode With Single Faults Imposed." *Applied Engineering*, 29:770–78.
- Kim, W., and Braun, J.E. 2013. "Performance Evaluation of a Virtual Refrigerant Charge Sensor." *International Journal of Refrigeration*, 36:1130–41.
- Osborne, W.C. 1977. *Fans*. 2nd edition. London: Pergamon Press.
- Reddy, T.A. 2007. "Formulation of a Generic Methodology for Assessing FDD Methods and Its Specific Adoption to Large Chillers." *ASHRAE Transactions*, 113(2):334–42.
- Rice, C.K. 1987. "The Effect of Void Fraction Correlation and Heat Flux Assumption on Refrigerant Charge Inventory Predictions." *ASHRAE Transactions*, 93(1):341–67.
- Rossi, T.M. 1995. *Detection, Diagnosis, and Evaluation of Faults in Vapor Compression Cycle Equipment*. Ph.D. Thesis. West Lafayette, IN: Purdue University.
- Shen, B. 2006. *Improvement and Validation of Unitary Air Conditioner and Heat Pump Simulation Models at Off-Design Conditions*. Ph.D. Thesis. West Lafayette, IN: Purdue University.
- Shen, B., Braun, J.E., and Groll, E.A. 2011. "The Impact of Refrigerant Charge, Airflow, and Expansion Devices on the Measured Performance of an Air-Source Heat Pump—Part I." *ASHRAE Transactions*, 117(2):533.
- Usoro, P.B., Schick, I.C., and Negahdaripour, S. 1985. "An Innovation-Based Methodology for HVAC System Fault Detection." *Journal of Dynamic Systems, Measurement, and Control*, 107:284–89.
- Wang, S., and Qin, J. 2005. "Sensor Fault Detection and Validation of VAV Terminals in Air Conditioning Systems." *Energy Conversion and Management*, 46:2482–2500.
- Wang, S., Zhou, Q., and Xiao, F. 2010. "A System-Level Fault Detection and Diagnosis Strategy for HVAC Systems Involving Sensor Faults." *Energy and Buildings*, 42:477–90.
- Xiao, F., Zhao, Y., Wen, J., and Wang, S. 2014. "Bayesian Network Based FDD Strategy for Variable Air Volume Terminals." *Automation in Construction*, 41:106–11.

Yang, L., Braun, J.E., and Groll, E.A. 2007. “The Impact of Fouling on the Performance of Filter Evaporator Combinations.” *International Journal of Refrigeration*, 30:489–98.

Yang, M., Zhao, X., Li, H., and Wang, W. 2013. “A Smart Virtual Outdoor Air Ratio Sensor in Rooftop Air Conditioning Units.” *Applied Thermal Engineering*, doi: 10.1016/j.applthermaleng.2013.12.046.

Zhao, X., Yang, M., and Li, H. 2012. “A Virtual Condenser Fouling Sensor for Chillers.” *Energy and Buildings*, 52:68–76.

Zhao, Y., Xiao, F., Wen, J., Lu, Y., and Wang, S. 2014. “A Robust Pattern Recognition-Based Fault Detection and Diagnosis (FDD) Method for Chillers.” *HVAC&R Research*, 20(7):798–809.

Zhou, Q., Wang, S., and Ma, Z. 2009. “A Model-based Fault Detection and Diagnosis Strategy for HVAC Systems.” *International Journal of Energy Research*, 33(10):903–18.

## Appendix A: Review of Statistical Measures

In this appendix, the accuracy of the empirical models of faults with empirical parameters estimated from training data is assessed with two statistical measures. This section of the appendix reviews the two measures used in this report: coefficient of determination and maximum deviation.

Definitions of some variables are needed to review the statistical measures. They are  $y$ , which is the variable to be estimated by an empirical model,  $y_{train,i}$ , which is the variable values of the  $i^{\text{th}}$  data point in the training data,  $\bar{y}_{train}$ , which is the average value of  $y$  from the training data,  $\hat{y}_{train,i}$  which is the estimated value of  $y$  at the  $i^{\text{th}}$  data point by the empirical model, and  $n$ , which is the number of data points in the training data.

Coefficient of determination is widely known as  $r^2$  as its abbreviation. It is commonly used to evaluate the proportion of training data point that is interpreted by the empirical model. It is calculated using equation (A-1).

$$r^2 = 1 - \frac{\sum_{i=1}^n (\hat{y}_{train,i} - y_{train,i})^2}{\sum_{i=1}^n (y_{train,i} - \bar{y}_{train})^2} \quad (\text{A-1})$$

Maximum deviation is the maximum magnitude of the difference between the empirical model estimates and the corresponding variable in the training data. It is calculated using equation (A-2).

$$\text{Maximum deviation} = \max(\{|\hat{y}_{train,i} - y_{train,i}| \mid \forall i \in [1, n]\}) \quad (\text{A-2})$$

## Appendix B: Control Faults

In this appendix, the modeling approaches and the verification results of the following three faults related to the control algorithm of the building equipment are discussed:

- No setback of thermostat set point in unoccupied hours
- Extended morning or evening thermostat set points
- Manual change of thermostat set point due to extreme outside temperature.

Because the MEC is the only building model with changes in thermostat set point with time in this study, it is used to verify the first two fault models. The third fault model is verified with the SEB model. The normal control schemes are also assumed to be those in the calibrated building models.

### B.1 No Setback of Thermostat Set Point in Unoccupied Hours

This control fault occurs when building managers accidentally use a constant set point at all times rather than set points that result in less energy consumption during unoccupied hours. In normal cases, building managers use a lower cooling thermostat set point and higher heating set point in occupied hours than unoccupied hours, because (1) keeping the building very comfortable during unoccupied hours is unnecessary, and (2) using different set points reduces the building load. This fault is modeled by changing the thermostat set point of unoccupied hours every day to its occupied value. If the building has multiple thermostat set points during the occupied hours, the thermostat set point immediately prior to building closure will replace the set point in the unoccupied hours to model the fault.

Because the fault leads the building to be controlled with a lower cooling thermostat set point and a higher heating thermostat set point on average, a building with this fault is expected to consume more electricity and gas. To verify the model, the fault model was applied to all thermostats in the MEC model in 2012, and the simulation results are compared with the normal case in Table B-1.

**Table B-1. Changes in MEC Building Performance with No Setback Fault**

	<b>Changes in Electricity Consumption from Nonfaulted Case (%)</b>	<b>Changes in Gas Consumption from Nonfaulted Case (%)</b>
<b>Chiller and cooling tower</b>	+0.0	N/A (Not available)
<b>Blower in the indoor air ducts</b>	+3.6	N/A
<b>Gas boiler</b>	N/A	+1.6
<b>Pumps for water flow in the chiller, cooling tower, and boiler</b>	+0.0	N/A
<b>Overall</b>	+0.1	+1.6

The gas consumption results in Table B-1 are the same as the expected increase in energy consumption. However, the chiller and the cooling tower electricity use changes little with the fault. An inspection of the simulated AHU VAV box damper positions shows that the dampers were maintained at their minimum positions during most of the cooling season, and the zone temperatures were much lower than the cooling thermostat set point. Thus, changing the thermostat set point did not change the electricity consumption of the chiller and the cooling tower significantly. In a location such as Florida, where the evening ambient temperature is higher than in Golden, Colorado, the use of daytime thermostat cooling set point at night may significantly increase the building load in the evening and the energy consumption of the chiller and cooling tower, and the results in Table B-1 may become more significant.

## B.2 Extended Morning and Evening Thermostat Set Point

This model assumes that the building model has a design schedule for precooling or preheating the building according to the occupancy schedule, but the building manager has extended the set point further to the unoccupied hours and may induce extra energy consumption without improving thermal comfort. For example, the building equipment design schedule is from 7 a.m. to 6 p.m., and the building manager accidentally put the thermostat set point schedule of the occupied hours from 6 a.m. to 7 p.m. This is the extended morning and evening thermostat set point fault if thermal comfort during occupancy after the extension is not improved.

To model the extension of the thermostat schedule, the first change of thermostat set point of the day is assumed to be the time when preheating or precooling happens or the opening of the building, whichever comes earlier, and the last change of thermostat set point of the day is caused by the closing of the building. The extended morning thermostat set point can be modeled by shifting the first change of thermostat set point to an earlier time. Likewise, the fault of extended evening thermostat set point can be modeled by shifting the last change of thermostat set point to a later time of the day.

The annual simulation results of the MEC model after imposing the extension of morning and evening thermostat set point in all zones are tabulated in Table B-2 and Table B-3.

**Table B-2. Changes in MEC Building Performance with Extended Morning Set Point for 3 Hours**

	<b>Changes in Electricity Consumption from Original Case (%)</b>	<b>Changes in Gas Consumption from Original Case (%)</b>
<b>Chiller and cooling tower</b>	+0.0	N/A
<b>Blower in the indoor air ducts</b>	+1.2	N/A
<b>Gas boiler</b>	N/A	+0.6
<b>Pumps for water flow in the chiller, cooling tower, and boiler</b>	+0.0	N/A
<b>Overall</b>	+0.03	+0.6

**Table B-3. Changes in MEC Building Performance with Extended Evening Set Point for 3 Hours**

	<b>Changes in Electricity Consumption from Original Case (%)</b>	<b>Changes in Gas Consumption from Original Case (%)</b>
<b>Chiller and cooling tower</b>	+0.0	N/A
<b>Blower in the indoor air ducts</b>	+0.6	N/A
<b>Gas boiler</b>	N/A	+0.1
<b>Pumps for water flow in the chiller, cooling tower, and boiler</b>	+0.0	N/A
<b>Overall</b>	+0.02	+0.1

The results in Table B-2 and Table B-3 show that electricity and gas consumption increase because of the extension, and the increases are smaller than those in Table B-1. This is expected, because the extended morning and evening thermostat set point fault is a change of thermostat set point in between the nonfaulted case and the no evening setback fault. If the extension period is stretched to cover all the unoccupied hours, it will become the no evening setback fault.

Because the thermostat set point schedule in the building model may not be optimized for precooling and preheating, an extension of thermostat set point to the morning may help to improve occupants' thermal comfort by precooling and preheating the building before occupancy. To determine if the extension is a fault, the number of days thermal comfort is reached in the first hour of building occupancy is examined. The comparison shows that the extension improves the thermal comfort in the building for 6 days, and the extension of morning thermostat set point for 3 hours is not a fault for this building.

### **B.3 Manual Change of Thermostat Set Point Due to Extreme Ambient Temperature**

This fault is caused by a manual override of thermostat set point on days with extreme outside temperatures. During very hot days or cold days, occupants may find the indoor temperature insufficient to warm or cool them as quickly as they would like when they enter the building, and they may override the thermostat set point by adjusting it to be hotter or cooler. Although the original schedule is sufficient to reach the building load with minimal energy consumption, occupants would like to achieve thermal comfort a few minutes sooner by overriding an optimized thermostat set point schedule. If the occupants do not reset the thermostat set point schedule after achieving their thermal comfort, it may significantly increase the energy consumption and may result in a fault.

No statistics are available about the outside temperature that will trigger occupants to change their thermostat set point, and this fault is modeled by assuming that occupants will reduce the cooling thermostat set point when the outside temperature is above a user-defined value. Likewise, when the outside temperature drops below a certain user-defined value, the occupants will presumably raise the heating thermostat set point. If the change causes the cooling thermostat set point to be lower than the heating thermostat set point, the simulation program

will use the heating set point as the zone thermostat set point. If the change causes the heating thermostat set point to be higher than the cooling thermostat set point, the simulation program will use the heating set point as the zone thermostat set point.

An annual simulation result of the SEB under this fault is shown in Table B-4 and Table B-5.

**Table B-4. Changes in MEC Building Performance with Manual Reduction of Cooling Thermostat Set Point by 4K When Temperature Is Higher Than 30°C**

	<b>Changes in Electricity Consumption from Nonfaulted Case (%)</b>	<b>Changes in Gas Consumption from Nonfaulted Case (%)</b>
<b>Compressor and condenser fan of the split system</b>	+8.9	N/A
<b>Blower in the indoor air ducts</b>	+0.0	N/A
<b>Gas furnace</b>	N/A	+0.0
<b>Overall</b>	+0.7	+0.0

**Table B-5. Changes in MEC Building Performance with Manual Increase of Heating Thermostat Set Point by 4K when Temperature Is Lower Than 5°C**

	<b>Changes in Electricity Consumption from Nonfaulted Case (%)</b>	<b>Changes in Gas Consumption from Nonfaulted Case (%)</b>
<b>Compressor and condenser fan of the split system</b>	+0.0	N/A
<b>Blower in the indoor air ducts</b>	+0.0	N/A
<b>Gas furnace</b>	N/A	+31.3
<b>Overall</b>	+0.0	+31.3

Table B-4 and Table B-5 show results that follow expectation. When the cooling thermostat set point is reduced manually, the electricity consumption for cooling (compressor and condenser fan) increases. When the heating thermostat set point is raised manually, the heating energy consumption (gas consumption in gas furnace) increases.

## Appendix C: Sensor Faults

This appendix describes models of sensor bias faults and their results. When a sensor ages, its measurement results may drift from its calibration result. If the sensor is not recalibrated, the drift may significantly affect the building performance. This section describes the modeling of three types of sensor bias:

- Economizer relative humidity sensor bias
- Temperature sensor bias along water circuits
- Supply air temperature sensor bias.

### C.1 Economizer Relative Humidity Sensor Bias

Relative humidity sensors are installed only in economizers that are controlled according to the air-water enthalpy of the outdoor air and return air. The economizer control algorithm converts the temperature and relative humidity sensor readings into air-water enthalpy values in controlling the damper position. A positively biased relative humidity sensor will increase the air-water enthalpy estimated by the control algorithm. If the control algorithm closes the damper when the air-water enthalpy of return air is lower than that of the ambient air and the return air relative humidity is positively biased, the damper will open in some cases when the actual return air-water enthalpy of ambient air is higher than that of the return air. The air-water enthalpy entering the cooling equipment will hence be higher than the normal condition, leading to higher energy consumption of the cooling equipment. A similar situation will occur if the ambient air relative humidity sensor is negatively biased.

To model humidity sensor bias, the economizer model was configured to shift the relative humidity values according to the bias before the calculation of the air-water enthalpy values. For instance, if there is a +2% sensor bias of the ambient air relative humidity sensor and the ambient air relative humidity is 32%, the fault model will pass the increased ambient air relative humidity value of 34% to the economizer model so it determines the damper opening.

The model was verified with the MEC model with relative humidity sensor models imposed on the economizer model of all three AHUs. The results are shown in Table C-1 and Table C-2.

**Table C-1. Changes in MEC Building Performance with Return Air Relative Humidity Sensor Bias +3%**

	<b>Changes in Electricity Consumption from Nonfaulted Case (%)</b>	<b>Changes in Gas Consumption from Nonfaulted Case (%)</b>
<b>Chiller and cooling tower</b>	+13.6	N/A
<b>Blower in the indoor air ducts</b>	+48.7	N/A
<b>Gas boiler</b>	N/A	+0.9
<b>Pumps for water flow in the chiller, cooling tower, and boiler</b>	-0.2	N/A
<b>Overall</b>	+11.5	+0.9

**Table C-2. Changes in MEC Building Performance with Ambient Air Relative Humidity Sensor Bias -3%**

	Changes in Electricity Consumption from Nonfaulted Case (%)	Changes in Gas Consumption from Nonfaulted Case (%)
Chiller and cooling tower	+12.2	N/A
Blower in the indoor air ducts	+50.9	N/A
Gas boiler	N/A	+0.8
Pumps for water flow in the chiller, cooling tower, and boiler	-0.2	N/A
Overall	+12.2	+0.8

Table C-1 and Table C-2 show that the cooling equipment uses much more energy to cool the zones than the nonfaulted case when the relative humidity sensor bias occurs. The bias also increases the energy consumption of the blowers as the equipment runs longer to meet the cooling thermostat set point. To determine whether the positive return air relative humidity sensor bias and negative outdoor air relative humidity sensor bias increase airflow from outdoors, the time profiles of the outdoor air mass flow rates through the damper in these two faulted cases are compared to that of the nonfaulted condition shown in Figure C-1.

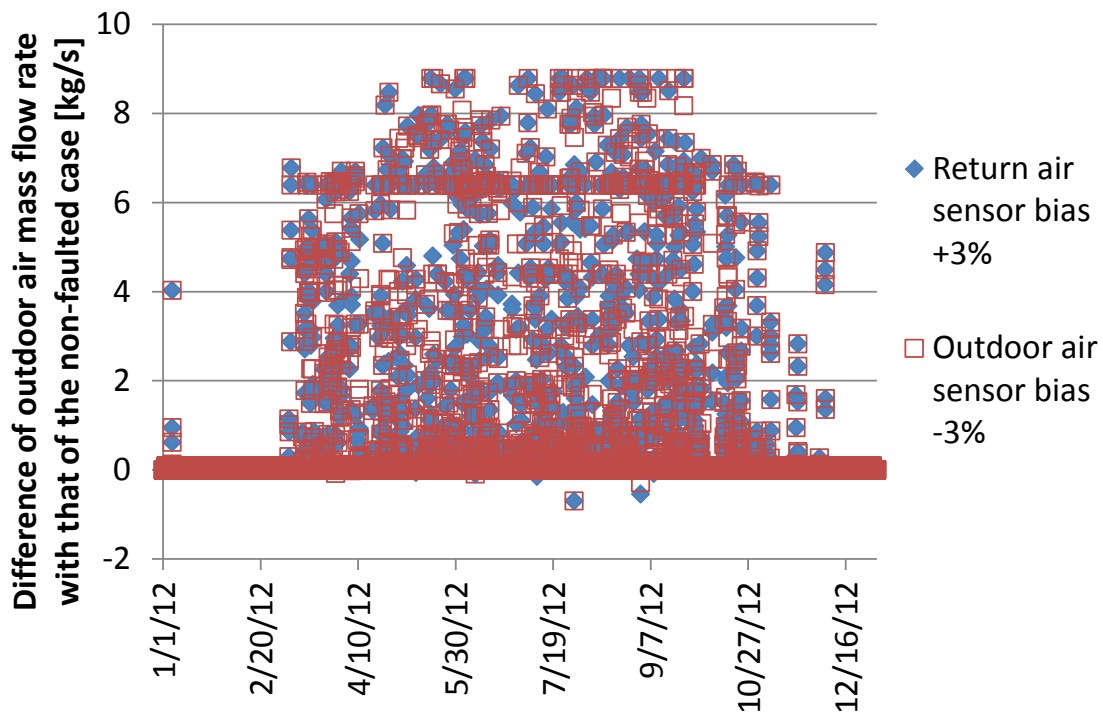


**Figure C-1. Difference in the outdoor air mass flow rate through the economizer damper between cases with relative humidity sensor bias and the nonfaulted case**

Figure C-1 shows that the outdoor air mass flow rates in the faulted cases are on average higher than those of the nonfaulted case despite occasionally lower air mass flow rate in transient operation. This meets the authors' expectation of the effect of the relative humidity sensor bias.

## C.2 Temperature Sensor Bias along Water Circuits

A temperature sensor bias may happen along the water circuits supplying hot or chilled water to the AHUs or water circuits between chillers and cooling towers if the temperature sensors are not calibrated regularly. These sensors are mainly used to control the water supply temperature from the chillers, cooling towers, and furnaces. If a positive bias occurs at the chiller water outlet, the faulted sensor will give a reading higher than the real temperature, and the chiller will eventually control the water outlet temperature to be lower than its control set point.

The bias cannot be modeled the same way as the economizer sensor bias models. Unlike the economizer relative humidity sensor bias, the water temperature reading at the water circuits may be passed to multiple component models. Modeling the bias by shifting the temperature input of all models that use the reading is inefficient. Changing the temperature record at the sensor location in the simulation program is invalid, because it changes the record of the real temperature and affects the mass conservation and heat transfer calculation incorrectly. To avoid changing the real temperature record, the bias was modeled by changing the set point configuration in the simulation program the same way as the thermostat bias fault in Basarkar et al. (2011), where the temperature set point at the sensor is reduced by the positive bias of the sensor. For instance, if the temperature sensor reads 2K lower than normal, the model increases the temperature set point at the sensor location by 2K.

The fault was imposed for the temperature sensor at the evaporator water outlet of the chiller in the MEC model to verify the model. The simulation results are tabulated in Table C-3 and Table C-4.

**Table C-3. Changes in MEC Building Performance with Temperature Sensor Bias +3K at chiller evaporator water outlet**

	<b>Changes in Electricity Consumption from Nonfaulted Case (%)</b>	<b>Changes in Gas Consumption from Nonfaulted Case (%)</b>
<b>Chiller and cooling tower</b>	+0.7	N/A
<b>Blower in the indoor air ducts</b>	+0.0	N/A
<b>Gas boiler</b>	N/A	+0.0
<b>Pumps for water flow in the chiller, cooling tower, and boiler</b>	+0.0	N/A
<b>Overall</b>	+0.5	+0.0

**Table C-4. Changes in MEC Building Performance with Temperature Sensor Bias  
–3K at Chiller Evaporator Water Outlet**

	<b>Changes in Electricity Consumption from Nonfaulted Case (%)</b>	<b>Changes in Gas Consumption from Nonfaulted Case (%)</b>
<b>Chiller and cooling tower</b>	–0.6	N/A
<b>Blower in the indoor air ducts</b>	+0.0	N/A
<b>Gas boiler</b>	N/A	+0.0
<b>Pumps for water flow in the chiller, cooling tower, and boiler</b>	+0.0	N/A
<b>Overall</b>	–0.4	+0.0

The results in Table C-3 and Table C-4 follow the expectation that a positive sensor bias at the chiller outlet increases the energy consumption of cooling equipment and vice versa when the bias is negative.

### **C.3 Supply Air Temperature Sensor Bias**

Positively biased supply air temperature sensors can cause the AHU to deliver air at a temperature lower than the supply air temperature set point. This can reduce the airflow in the cooling season and increase the airflow in the heating season to reach the zone thermostat set point. If the required cooling airflow falls below the minimum airflow of the AHUs, it will increase the use of reheat or the zone temperature will fall out of control.

The modeling approach of this fault is the same as the water temperature sensor bias. If the sensor is biased by –2K, the set point at the supply air is increased by 2K to model the fault.

The model was verified with the simulation results of imposing supply air temperature sensor bias for all AHUs in the MEC model. Results are shown in Table C-5.

**Table C-5. Changes in MEC Building Performance with Temperature Sensor Bias  
+2K at the Supply Air of All AHUs**

	<b>Changes in Electricity Consumption from Nonfaulted Case (%)</b>	<b>Changes in Gas Consumption from Nonfaulted Case (%)</b>
<b>Chiller and cooling tower</b>	+14.5	N/A
<b>Blower in the indoor air ducts</b>	+0.2	N/A
<b>Gas boiler</b>	N/A	–7.3
<b>Pumps for water flow in the chiller, cooling tower, and boiler</b>	+6.5	N/A
<b>Overall</b>	+11.2	–7.3

To examine the decrease of gas consumption due to the bias, the differences of gas consumption and total air mass flow rate from the AHUs on a weekday (January 16, 2012) are plotted in Figure C-2.

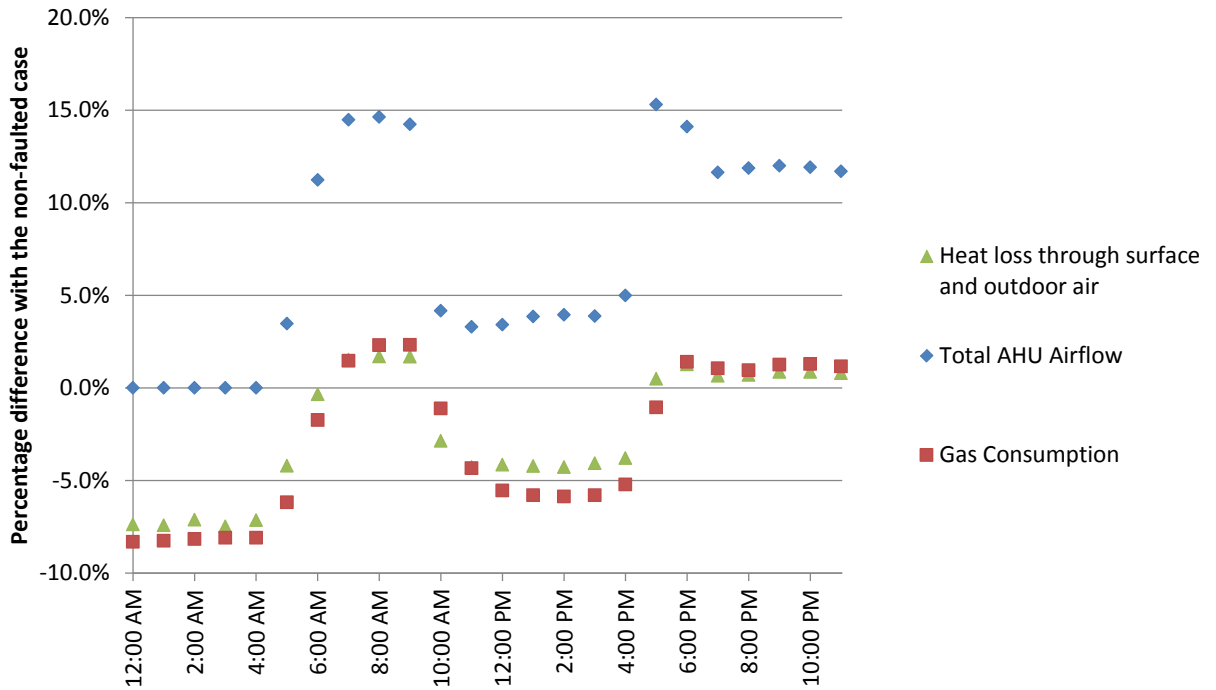


**Figure C-2. Difference in gas consumption, AHU air mass flow rate, and building heat loss between the case with supply air temperature bias at +2K and the nonfaulted case on a weekday during the heating season on January 4, 2012**

Figure C-2 shows a time in the beginning of the day when the AHU airflows are equal. That is the time when the airflows were maintained at their minimum because the required airflow rates to reach the thermostat set point were lower than the minimum AHU airflow. At this time, a lower supply air temperature would decrease the delivered heat and lower the gas consumption. This results in a lower zone temperature in the beginning of the day as shown in Figure C-3.

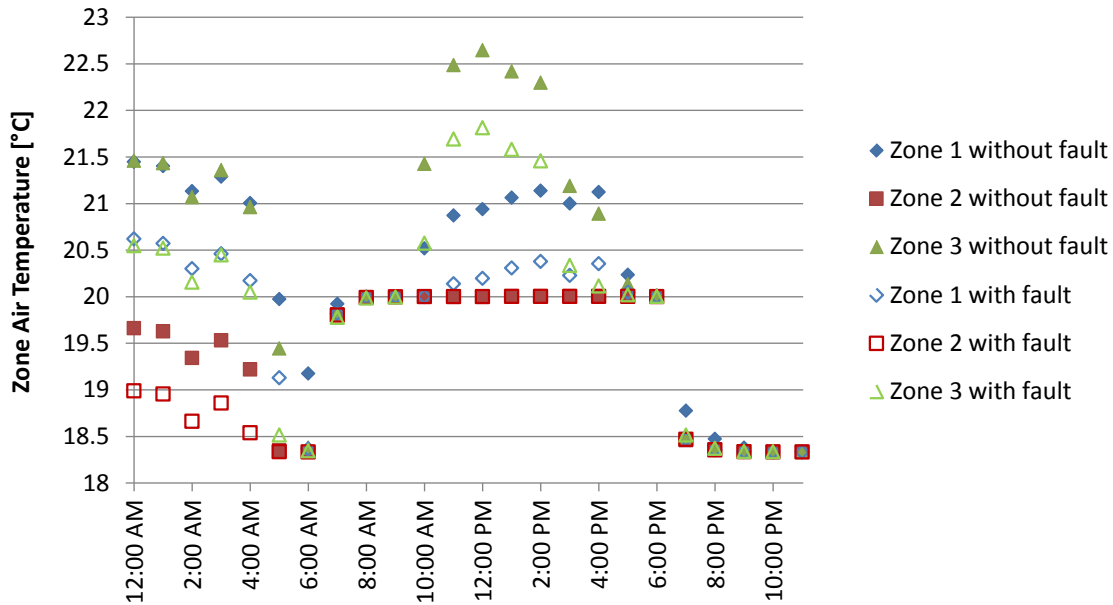


**Figure C-3. Zone air temperature of the case with supply air temperature bias at +2K and the nonfaulted case on a weekday during the heating season on January 4, 2012**

Figure C-3 shows that the bias and the minimum airflow operation cause the zone air temperature to be lower in all zones. The gas consumption of the faulted case is thus lower than the nonfaulted case.

After 4 a.m., the AHU airflows of the two cases differed because a higher airflow was needed in some of the zones to meet the heating requirement, which is illustrated by some equal zone temperatures of the faulted and nonfaulted cases after 4 a.m. in Figure C-3. The gas consumption of the faulted case was slightly higher than the nonfaulted case to compensate for the difference in building heat loss in Figure C-2 that follows the change in gas consumption. The higher heat loss of the faulted case in Figure C-2 was a result of its lower zone surface temperature, and its building walls required more heat and longer time than the nonfaulted case to reach steady state. If the zone air temperature is maintained at the thermostat set point for sufficient time, the zone surface temperature and hence the gas consumption of the faulted case will be the same as that of the nonfaulted case. In the cooling season, the AHU VAV box dampers were maintained at their minimum position in both faulted and nonfaulted conditions because the chiller and the cooling tower were oversized. The cooling delivered to the zones depended on the supply air temperature only such that a lower supply air temperature resulted in more cooling and hence more electricity use from the chiller and the cooling tower. In this case, the faulted AHUs delivered air at a lower supply air temperature because of the sensor bias, and hence the chiller and the cooling tower of the faulted building consumed more electricity than the nonfaulted case as shown in Table C-5.

## Appendix D: Rooftop Unit and Split Air Conditioner Fault

This appendix describes fault models that directly affect the empirical component model of RTUs and split air conditioners in EnergyPlus. EnergyPlus uses the DOE-2 DX cooling coil model (Brandemuehl et al. 1993) to estimate the total cooling capacity and the electrical power consumption of the compressor and condenser fan of single-speed DX coils by equations (D-1) to (D-7).

$$\dot{Q}_{cool,dx} = \dot{Q}_{cool,dx,rat} f_1(T_{wb,ent}, T_{db,amb}) f_2\left(\frac{\dot{m}_a}{\dot{m}_{a,rat}}\right) \quad (D-1)$$

$$\begin{aligned} f_1(T_{wb,ent}, T_{db,amb}) \\ = a_0 + a_1 T_{wb,ent} + a_2 T_{wb,ent}^2 + a_3 T_{db,amb} + a_4 T_{db,amb}^2 \\ + a_5 T_{wb,ent} T_{db,amb} \end{aligned} \quad (D-2)$$

$$f_2\left(\frac{\dot{m}_a}{\dot{m}_{a,rat}}\right) = a_6 + a_7 \left(\frac{\dot{m}_a}{\dot{m}_{a,rat}}\right) \quad (D-3)$$

$$EIR_{dx} = \frac{\dot{W}_{dx}}{\dot{Q}_{cool,dx}} \quad (D-4)$$

$$\frac{EIR_{dx}}{EIR_{dx,rat}} = f_3(T_{wb,ent}, T_{db,amb}) f_4\left(\frac{\dot{m}_a}{\dot{m}_{a,rat}}\right) \quad (D-5)$$

$$\begin{aligned} f_3(T_{wb,ent}, T_{db,amb}) \\ = a_8 + a_9 T_{wb,ent} + a_{10} T_{wb,ent}^2 + a_{11} T_{db,amb} + a_{12} T_{db,amb}^2 \\ + a_{12} T_{wb,ent} T_{db,amb} \end{aligned} \quad (D-6)$$

$$f_4\left(\frac{\dot{m}_a}{\dot{m}_{a,rat}}\right) = a_{14} + a_{15} \left(\frac{\dot{m}_a}{\dot{m}_{a,rat}}\right) \quad (D-7)$$

The power consumption of the compressor and condenser fan was modeled using the energy input ratio in EnergyPlus as shown in equation (D-4). The sensible heat ratio of the evaporator was modeled using the bypass factor model as shown in equations (D-8) to (D-11),

$$BF = e^{-UA_{rat}/\dot{m}_a c_{p,a}} \quad (D-8)$$

$$h_{adp} = h_{ent} - \frac{h_{ent} - h_{lvg}}{1 - BF} \quad (D-9)$$

$$\omega_{lvg} = \omega_{adp} + BF(\omega_{ent} - \omega_{adp}) \quad (D-10)$$

$$SHR = \frac{h(T_{ent}, \omega_{adp}) - h_{adp}}{h_{ent} - h_{adp}} \quad (D-11)$$

The calculation starts by solving all equations with the current wet-bulb temperature at the air inlet of the evaporator of the DX cooling coil. If the resultant sensible heat ratio is smaller than 1, the result is accepted and the evaporator coil is estimated to be wet. Otherwise, a wet-bulb temperature at the evaporator inlet is solved from equations (D-8) to (D-11) so that sensible heat ratio from equation (D-11) is 1, and this wet-bulb temperature is used to solve the total cooling capacity and power consumption in equations (D-1) and (D-5). This extra step gives the solution when the evaporator coil is dry.

Equations (D-1) to (D-11) show that the refrigerant system and the condenser fan are modeled empirically and there are no physical parameters for directly imposing faults. To model the effect of faults on total cooling capacity, power consumption of compressor and condenser fan, and sensible heat ratio, equations (D-12) to (D-14) were developed in this project.

$$\frac{\dot{Q}_{cool,dx,F}}{\dot{Q}_{cool,dx}} = 1 + F \left\{ c_{F,0} + c_{F,1} \left( \frac{T_{wb,ent}}{273.15[K]} + 1 \right) + c_{F,2} \left( \frac{T_{db,amb}}{273.15[K]} + 1 \right) + c_{F,3} F \right. \\ \left. + c_{F,4} F^2 + c_{F,5} \frac{\dot{Q}_{cool,dx,rat}}{\dot{W}_{dx,rat}} \right\} \quad (D-12)$$

$$\frac{EIR_{dx,F}}{EIR_{dx}} = 1 + F \left\{ c_{F,6} + c_{F,7} \left( \frac{T_{wb,ent}}{273.15[K]} + 1 \right) + c_{F,8} \left( \frac{T_{db,amb}}{273.15[K]} + 1 \right) + c_{F,9} F \right. \\ \left. + c_{F,10} F^2 + c_{F,11} \frac{\dot{Q}_{cool,dx,rat}}{\dot{W}_{dx,rat}} \right\} \quad (D-13)$$

$$UA_{rat,F} = (1 + c_{F,12} F) UA_{rat} \quad (D-14)$$

The ratios on the left side of equations (D-12) and (D-13) are called *fault impact ratios* because they describe the change of the air conditioner performance due to faults.

Equations (D-12) and (D-13) adjust the cooling capacity and power consumption of the air conditioner model according to the fault level, and equation (D-14) adjusts the rated heat transfer conductance in the bypass factor model equation (D-8) to model the effects of faults on the sensible heat ratio. These three equations were constructed following the idea in Cho et al. (2014) such that when the fault level  $F$  is zero, the equations do not change the building model.

Although equations (D-12) to (D-14) can easily be combined with the original empirical models of the air conditioner, they contain empirical parameters that need training data to estimate. These training data were obtained by conducting simulation with the models of multiple RTUs and split systems from Cheung and Braun (2013). The environmental conditions and the system specification for the training data are listed in Table D-1 and Table D-2.

**Table D-1. Environmental Conditions in Training Data of Empirical Models of Faulted Performance of RTUs and Split Systems**

Environmental Condition	Values
Dry-bulb temperature at air inlet of evaporator (°C)	21.1, 22.8, 24.4, 26.1, 27.8, 29.4
Wet-bulb temperature at air inlet of evaporator (°C)	12.8, 15.6, 18.3, 21.1, 23.9
Outdoor air dry-bulb temperature (°C)	18.3, 21.1, 23.9, 26.7, 29.4, 32.2, 35, 37.8, 40.6, 46.1

**Table D-2. System Specification in Training Data of Empirical Models of Faulted Performance of RTUs and Split Systems**

Index	Type of System	Compressor Type	Expansion Valve Type	Size (ton)	Refrigerant	Ratio of Rated Cooling Capacity to Power Consumption
RTU 1	Packaged	Scroll	Fixed orifice	3	R410A	4.69
RTU 2	Packaged	Scroll	Fixed orifice	5	R407C	3.74
Split 1	Split	Scroll	Thermostatic expansion valve	2.5	R410A	7.06
Split 2	Split	Scroll	Thermostatic expansion valve	3	R410A	5.11
Split 3	Split	Scroll	Fixed orifice	3	R22	5.70

Because the wet-bulb temperature used in the evaporator model differs from the true wet-bulb temperature for cases with a dry evaporator coil, only simulation results with wet evaporator coils were used as training data. The definition of the fault levels and the ranges of fault levels in the training data are described in later subsections that discuss the modeling results of various types of faults. The faults considered are listed below.

- Undercharged RTUs and split systems
- Condenser fouling in RTUs and split systems
- Condenser fan motor efficiency degradation in RTUs and split systems
- Liquid line restriction in RTUs
- Noncondensable entrainment in refrigerant flow in RTUs.

Although Section 5 includes no RTUs in the building models, because EnergyPlus uses identical mathematical tools (DOE-2 model) to model the cooling component of RTUs and split systems, all fault models in this section were verified with the SEB model.

## D.1 Undercharged Rooftop Units and Split Air Conditioners

If RTUs and split air conditioners are undercharged, it is usually because refrigerant has leaked from the refrigerant circuit of the air conditioners. During their installation phase, refrigerant is usually charged into the air conditioners according to the manufacturer’s recommendation, and

the refrigerant circuits are usually checked to be leak-free before commissioning. However, after a long period of operation, the junctions of the refrigerant circuit may develop leaks.

When a refrigerant circuit is running with less refrigerant, the average refrigerant density in the refrigerant circuit drops and it runs with more refrigerant vapor. This reduces the density of refrigerant at the compressor suction and expansion valve inlet and hence the refrigerant mass flow rate and the cooling capacity of the circuit. The reduction also induces a lower evaporating pressure and temperature in the circuit, which lead to more water condensation on the evaporator coil and lower sensible heat ratio. The lower evaporating pressure and greater superheat entering the compressor lead to greater power consumption.

The refrigerant charge fault level is defined as the percentage loss of the amount of refrigerant from the air conditioner relative to the manufacturer’s recommendation. It is zero when no refrigerant has leaked out of the system, and it is one when all the refrigerant is lost from the system.

The empirical coefficients in equations (D-12) to (D-14) were trained with the RTU and split air conditioner data in Table D-2 with a range of fault level of 0% to 30% by linear regression. The results are tabulated in Table D-3.

**Table D-3. Statistics of the Estimation Results of Fault Models for Undercharged RTUs and Split Air Conditioners**

Type of System	Estimated Value	$r^2$	Maximum Deviation
<b>RTU</b>	Fault impact ratio of cooling capacity	0.9754	0.04
	Fault impact ratio of energy input ratio	0.9302	0.05
	Sensible heat ratio	0.9963	0.06
<b>Split air conditioner</b>	Fault impact ratio of cooling capacity	0.9468	0.05
	Fault impact ratio of energy input ratio	0.8629	0.07
	Sensible heat ratio	0.9718	0.09

Table D-3 shows a relatively low coefficient of determination for fault impact ratios of energy input ratios for split air conditioners. This is further studied by examining the parity plot of the fault impact ratio of power consumption in Figure D-1.

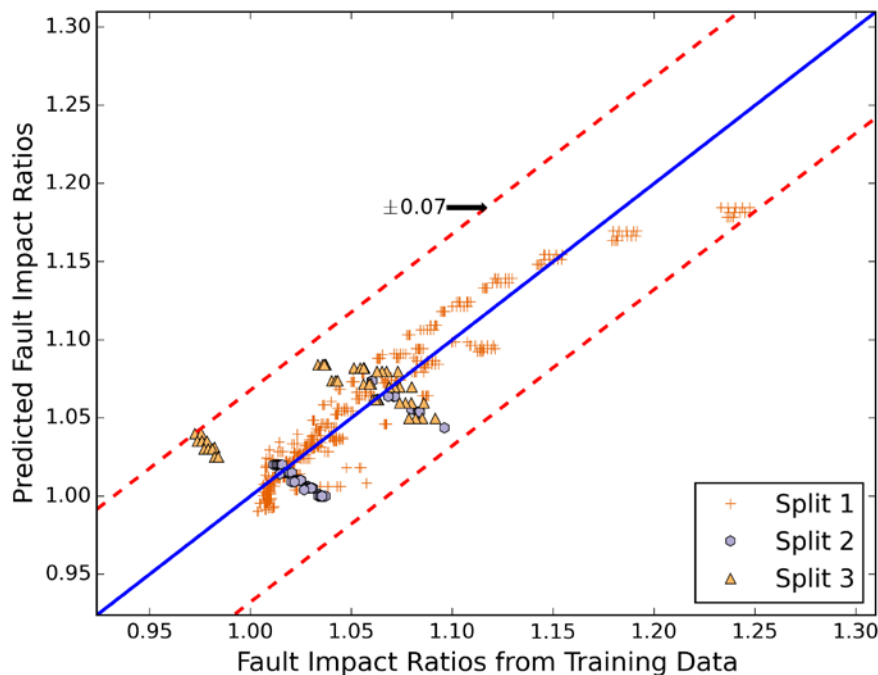


**Figure D-1. Comparison of fault impact ratios of energy input ratio of split air conditioners between the training data and prediction by empirical model for undercharging**

Figure D-1 shows that the fault impact ratios of two air conditioners span between 0.95 and 1.10 only, which is smaller than the range of the air conditioner Split 1. This creates a smaller denominator in the calculation of the coefficient of determination and a lower coefficient of determination.

To verify the fault model, the SEB model was used with the fault model, and the simulation results were studied as shown in Table D-4 and Table D-5.

**Table D-4. Change in Simulation Result of SEB Model Because of 30% Undercharging as Estimated by the RTU Undercharging Model**

	Changes in Electricity Consumption from Nonfaulted Case (%)	Changes in Gas Consumption from Nonfaulted Case (%)
Compressor and condenser fan of the split system	+9.9	N/A
Blower in the indoor air ducts	+0.0	N/A
Gas furnace	N/A	+0.0
Overall	+0.8	+0.0

**Table D-5. Change in Simulation Result of SEB Model Because of 30% Undercharging as Estimated by the Split Air Conditioner Undercharging Model**

	<b>Changes in Electricity Consumption from Nonfaulted Case (%)</b>	<b>Changes in Gas Consumption from Nonfaulted Case (%)</b>
<b>Compressor and condenser fan of the split system</b>	+13.4	N/A
<b>Blower in the indoor air ducts</b>	+0.0	N/A
<b>Gas furnace</b>	N/A	+0.0
<b>Overall</b>	+1.1	+0.0

The results in Table D-4 and Table D-5 are reasonable for undercharging models. When an air conditioner is undercharged, its cooling capacity and sensible heat ratio drop. The air conditioner needs to run longer to meet the sensible cooling demand in the building and is less efficient. The lower efficiency and lower sensible heat ratio lead to higher energy consumption by the cooling equipment as shown in Table D-4 and Table D-5.

## **D.2 Condenser Fouling in Rooftop Units and Split Air Conditioners**

Condensers in RTUs and split air conditioners are fouled by the accumulation of leaves, dirt, litter, etc. between the fins of the condenser located in an outdoor environment. Because the condenser fans of these air conditioners are usually single-speed, the pressure drop across the condenser increases and the condenser airflow drops. The reduced airflow causes higher condensing temperature and pressure. This increases the pressure difference across the compressor in the refrigerant circuit and the power consumption of the air conditioners.

According to Yang et al. (2007) and Bell et al. (2011), condenser fouling can be represented by the reduction of condenser airflow, and the fault level is defined as the percentage drop of airflow across the condenser due to fouling. For instance, when no airflow reduction is caused by condenser fouling, the fault level is zero. If condenser fouling causes a 30% drop of condenser airflow, the fault level of condenser fouling is 30%.

To build an empirical model of the fault impact of condenser fouling, training data were obtained by simulating the systems in Table D-2 with a condenser fouling level ranging from 0% to 50%. The simulation results showed that the sensible heat ratio changes due to condenser fouling are small and can be neglected. Figure D-2 shows example results for the small effect of condenser fouling on sensible heat ratio for Split 1.

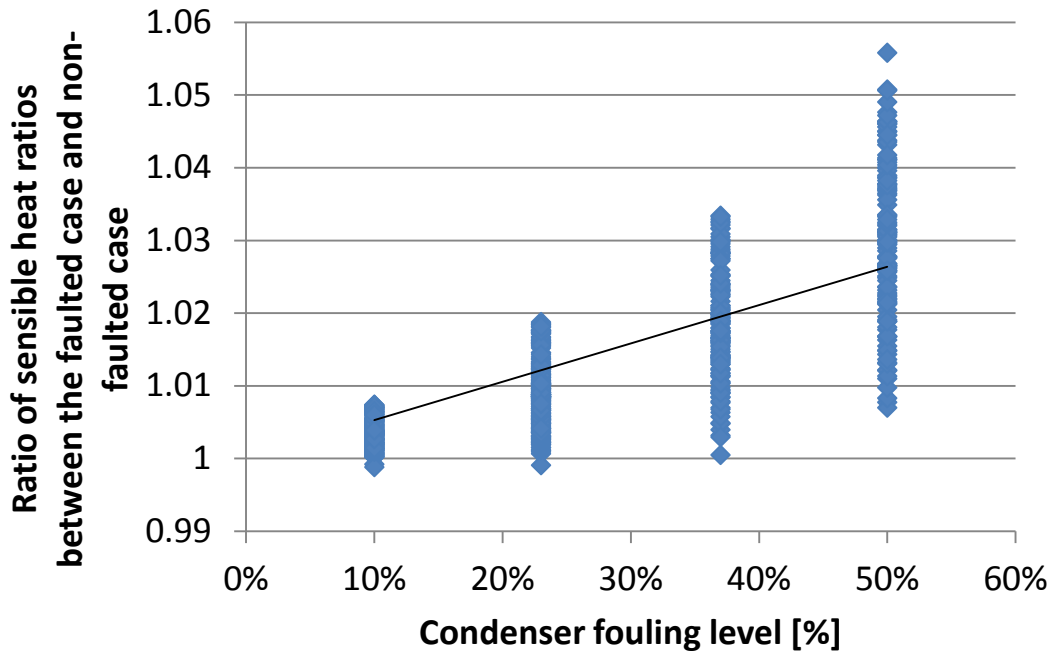


**Figure D-2. Changes in the ratios of sensible heat ratio between the condenser fouling case and nonfaulted case under different condenser fouling levels in air conditioner Split 1**

Figure D-2 shows that 50% condenser fouling changes the sensible heat ratio by only 3% on average, so this effect is not included in the fault modeling.

After estimating the coefficients of empirical models in equations (D-12) and (D-13) by linear regression with the training data, the estimation accuracies of the models were evaluated with statistical measures in Table D-6.

**Table D-6. Statistics of the Estimation Results of Condenser Fouling Models for RTUs and Split Air Conditioners**

Type of System	Estimated Value	$r^2$	Maximum Deviation
RTU	Fault impact ratio of cooling capacity	0.9662	0.06
	Fault impact ratio of energy input ratio	0.9802	0.16
Split air conditioner	Fault impact ratio of cooling capacity	0.9869	0.04
	Fault impact ratio of energy input ratio	0.9455	0.15

Table D-6 shows that the fault impact ratio estimation is accurate in general as reflected by the high coefficients of determinations. However, the maximum deviations of energy input ratios are high. The causes of the deviations are studied with the parity plots of the energy input ratios in Figure D-3 and Figure D-4.

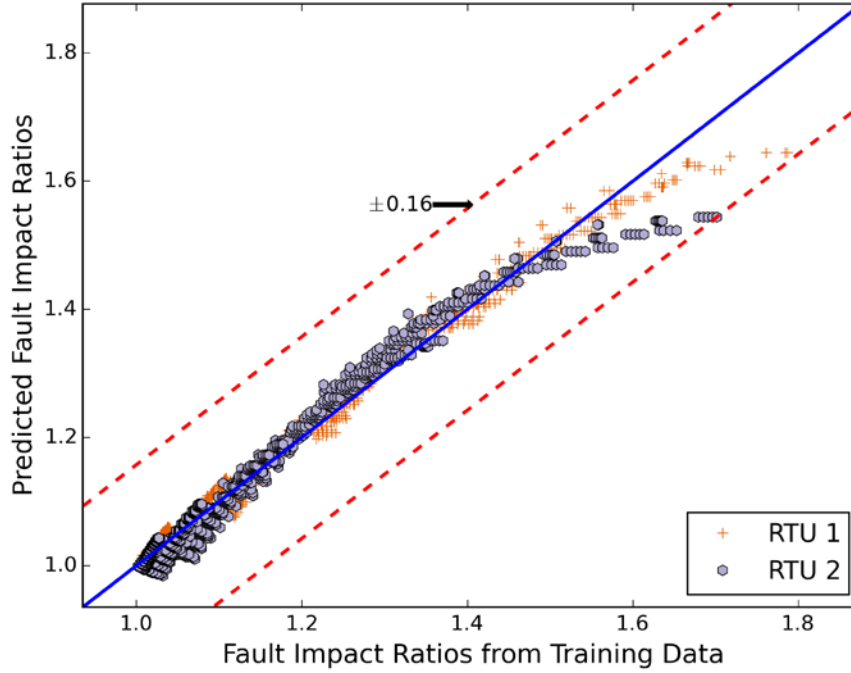


**Figure D-3. Comparison of fault impact ratios of energy input ratio of RTUs between the training data and prediction by empirical model for condenser fouling**

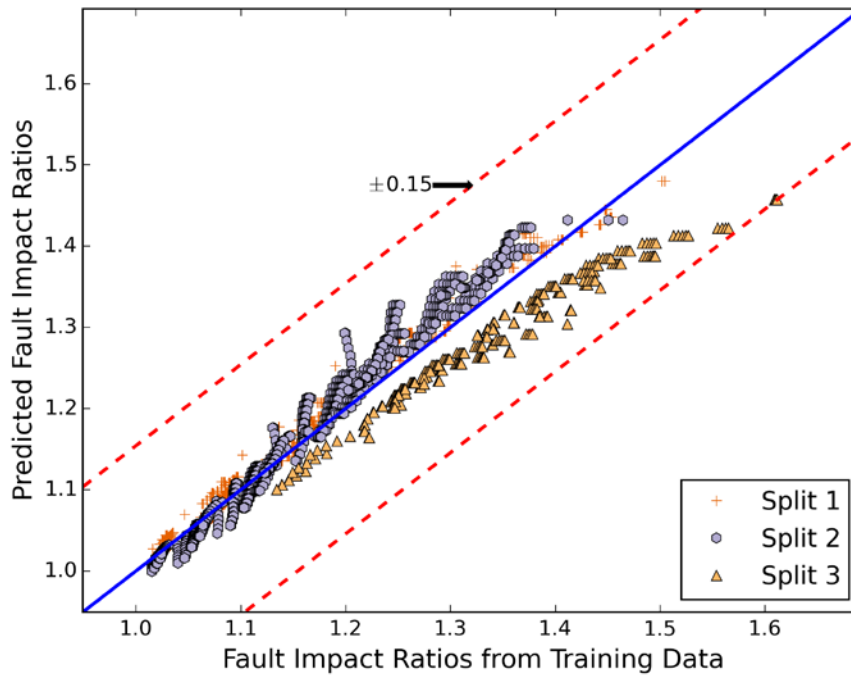


**Figure D-4. Comparison of fault impact ratios of energy input ratio of split air conditioners between the training data and prediction by empirical model for condenser fouling**

Figure D-3 shows that the high maximum deviation is caused by cases with fault impact ratios higher than 1.6. These scenarios were subjected to a condenser fouling level of 50%. The high maximum deviation for the fault model of RTUs is a result of a high fault level.

Figure D-4 shows a different pattern from Figure D-3. In Figure D-4, the fault impact ratios of system Split 3 were underestimated compared to the other two systems. This caused the maximum deviation 0.15 when the fault impact ratio was approximately 1.6. As the estimated value corresponds to the maximum fault level at 50%, the accuracy of the model is still acceptable.

To verify the condenser fouling models, both the RTU and split system fault models were used to simulate the condenser fouling impact in the split system of the SEB. The simulation results were tabulated in Table D-7 and Table D-8.

**Table D-7. Changes in Simulation Result of SEB Model Because of 50% Condenser Fouling as Estimated by the RTU Condenser Fouling Model**

	<b>Changes in Electricity Consumption from Nonfaulted Case (%)</b>	<b>Changes in Gas Consumption from Nonfaulted Case (%)</b>
<b>Compressor and condenser fan of the split system</b>	+18.3	N/A
<b>Blower in the indoor air ducts</b>	+0.0	N/A
<b>Gas furnace</b>	N/A	+0.0
<b>Overall</b>	+1.4	+0.0

**Table D-8. Changes in Simulation Result of SEB Model Because of 50% Condenser Fouling as Estimated by the Split Air Conditioner Fouling Model**

	<b>Changes in Electricity Consumption from Nonfaulted Case (%)</b>	<b>Changes in Gas Consumption from Nonfaulted Case (%)</b>
<b>Compressor and condenser fan of the split system</b>	+14.7	N/A
<b>Blower in the indoor air ducts</b>	+0.0	N/A
<b>Gas furnace</b>	N/A	+0.0
<b>Overall</b>	+1.1	+0.0

Table D-7 and Table D-8 show the expected result that the electricity consumption of compressor and condenser fan becomes higher than the nonfaulted case as the condenser is fouled.

### D.3 Liquid Line Restriction in Rooftop Unit

A liquid line restriction is caused by accumulation of particles in the filter along the refrigerant flow from the condenser to the expansion valve. The accumulation increases the flow resistance of the refrigerant circuit and the pressure difference across the compressor. The rise of the pressure difference results in higher compressor power consumption. The blockage can also induce accumulation of refrigerant in the condenser. Because the mass of refrigerant in the refrigerant circuit is constant, this reduces the mass of refrigerant in the evaporator and lowers the refrigerant density, pressure, and temperature in the evaporator. The reduction of refrigerant density lowers the compressor refrigerant mass flow rate and hence lowers evaporator heat transfer rate. The sensible heat ratio is also reduced by the reduction of evaporating temperature.

The definition of fault level of liquid line restriction follows the definition in Cheung and Braun (2013), which is the percentage difference from condenser outlet to evaporator inlet between the restriction case and the nonfaulted case. If the fault level is zero, there is no restriction. If the fault level is 25%, the pressure difference from the condenser outlet to evaporator inlet is 25% higher than that of the nonfaulted case.

At this stage of the project, only the liquid line restriction model for RTUs was constructed. The training data contained cases with restriction level ranging from 0% to 25% of the RTUs in Table D-2. The statistics of the accuracy of the model in equations (D-12), (D-13), and (D-14) were tabulated in Table D-9.

**Table D-9. Statistics of the Accuracy of the Liquid Line Restriction Model for RTUs**

<b>Estimated Value</b>	<b><math>r^2</math></b>	<b>Maximum Deviation</b>
<b>Fault impact ratio of cooling capacity</b>	0.9467	0.07
<b>Fault impact ratio of energy input ratio</b>	0.9720	0.05
<b>Sensible heat ratio</b>	0.9986	0.04

The coefficients of determination in Table D-9 are higher than 0.9, showing that the model accuracy is acceptable.

The model was verified by using the model to simulate the effect of liquid line restriction in the air conditioner in the SEB. The results are shown in Table D-10.

Table D-10 shows the liquid line restriction induces a higher electricity consumption of the compressor and condenser fan.

**Table D-10. Change in Simulation Result of SEB Model Because of 30% Liquid Line Restriction as Estimated by the RTU Liquid Line Restriction Fault Model**

	<b>Changes in Electricity Consumption from Nonfaulted Case (%)</b>	<b>Changes in Gas Consumption from Nonfaulted Case (%)</b>
<b>Compressor and condenser fan of the split system</b>	+17.4	N/A
<b>Blower in the indoor air ducts</b>	+0.0	N/A
<b>Gas furnace</b>	N/A	+0.0
<b>Overall</b>	+1.4	+0.0

## D.4 Noncondensable Entrainment in Refrigerant Flow in Rooftop Units

Air may enter the refrigerant circuit if the refrigerant circuit inner volume is not evacuated properly before the refrigerant is charged into the air conditioner. Because air cannot condense in the refrigerant circuit, it is typically trapped in the vapor section between the condenser and the compressor, and increases the refrigerant pressure of the condenser and the compressor. This forces the compressor to run with a higher refrigerant pressure and hence higher power consumption than normal operation.

Its fault level is defined as the ratio of the mass of the noncondensable in the refrigerant circuit to the mass of the noncondensable that the refrigerant circuit can hold under atmospheric pressure and temperature. The choice of the denominator of the fault level comes from Kim et al. (2009) so that the denominator represents the maximum mass of the noncondensable in an air conditioner in the field, which is a result of not extracting any air from the refrigerant circuit before refrigerant charging.

The empirical models of this fault using equations (D-12), (D-13), and (D-14) were obtained using training data from models of RTUs in Table D-2 with a range of fault level from 0% to 80%. The accuracy of the empirical model is assessed with the statistics in Table D-11.

**Table D-11. Statistics of the Accuracy of the Liquid Line Restriction Model for RTUs**

<b>Estimated Value</b>	<b><math>r^2</math></b>	<b>Maximum Deviation</b>
<b>Fault impact ratio of cooling capacity</b>	0.9214	0.06
<b>Fault impact ratio of energy input ratio</b>	0.9684	0.03
<b>Sensible heat ratio</b>	0.9971	0.05

Table D-11 shows that the coefficient of determination of the model is higher than 0.9 and the models are accurate enough to be used with building models.

The fault model was used to simulate the impact of noncondensable entrainment in refrigerant on the SEB, and the results are shown in Table D-12.

**Table D-12. Changes in Simulation Result of SEB Model Because of 60% Noncondensable Entrainment Fault as Estimated by the RTU Noncondensable Entrainment Fault Model**

	<b>Changes in Electricity Consumption from Nonfaulted Case (%)</b>	<b>Changes in Gas Consumption from Nonfaulted Case (%)</b>
<b>Compressor and condenser fan of the split system</b>	+10.1	N/A
<b>Blower in the indoor air ducts</b>	+0.0	N/A
<b>Gas furnace</b>	N/A	+0.0
<b>Overall</b>	+0.8	+0.0

Table D-12 shows that the noncondensable entrainment fault increases the building energy consumption by increasing the electricity use of the compressor and condenser fan.

## **D.5 Condenser Fan Motor Efficiency Degradation of Rooftop Units and Split Air Conditioners**

Condenser fan motor efficiency degradation is primarily the result of a motor bearing fault or stator winding fault (da Silva 2006).

A bearing fault is the deterioration of bearings around the motor shaft, which increases the friction of the shaft rotation. Although the increase of friction increases the motor torque, it has negligible effect on the rotational speed at its design condition. Because the torque of the motor increases and the motor rotational speed remains unchanged, the motor power consumption increases, and the constant rotational speed implies that the airflow of the fan remains unchanged. The bearing fault can hence be modeled by increasing the power consumption of the condenser fan only without changing the condenser fan airflow.

A stator winding fault can also be modeled in a similar manner. A stator winding fault is caused by short-circuiting of the stator winding inside the motor. According to Bouzid et al. (2013), a stator winding fault is equivalent to having an extra resistor installed in parallel with the stator winding circuit. Because the voltage applied to the motor is determined by the power source and remains unchanged by the fault, the extra resistor in parallel with the stator winding circuit draws extra current from the power source only and does not affect the operation of the rest of the circuit inside the motor. Because the electricity flow inside the motor rotor remains unchanged, the torque and speed of the motor rotation remain constant. Hence a stator winding fault can also be modeled as a fault that causes an increase of fan power consumption only without changing the airflow of the fan.

To model the fault, the fault level is first defined as the percentage reduction of motor efficiency. If the motor efficiency is 60% at the rated condition and the fault level is 10%, the motor efficiency becomes 54%. The equation to calculate the faulted motor power consumption from the normal motor power consumption can be written as equation (D-15).

$$\dot{W}_{fan,F} = \frac{\dot{W}_{fan}}{(1 - F)} \quad (D-15)$$

However, equation (D-15) cannot be imposed within the DX unit model in EnergyPlus directly because the model estimates the compressor and condenser fan power consumption together empirically. It is necessary to model the change of the condenser fan power consumption as a multiplier to the energy input ratio in equation (D-5). The multiplier can be derived by first recognizing the calculation of the compressor and condenser fan power consumption with the condenser fan motor degradation as equation (D-16).

$$\dot{W}_{cool,F} = \dot{W}_{cool} + \dot{W}_{fan,F} - \dot{W}_{fan} \quad (D-16)$$

Equations (D-15) and (D-16) can be combined to create equation (D-17).

$$\dot{W}_{cool,F} = \dot{W}_{cool} \left( 1 + \frac{\dot{W}_{fan}}{\dot{W}_{cool}} \left( \frac{F}{1 - F} \right) \right) \quad (D-17)$$

Since the cooling capacity of the air conditioner is not changed by the fault, the faulted energy input ratio can be written as equation (D-18).

$$\frac{EIR_F}{EIR} = 1 + \frac{\dot{W}_{fan}}{\dot{W}_{cool}} \left( \frac{F}{1 - F} \right) \quad (D-18)$$

Equation (D-18) gives a multiplier for the energy input ratio of the DX unit model to estimate the energy input ratio as a result of condenser fan motor efficiency degradation, but it still requires a ratio of condenser fan power consumption to the power consumption of compressor and condenser fan before it can be used. To estimate the ratio, the ratios of multiple RTUs and split air conditioners at their rated operating conditions were obtained and were averaged to estimate the ratio in equation (D-18). The specifications of the RTUs and split air conditioners used to get the average ratio are summarized in Table D-13.

**Table D-13. Summary of Specifications of Air Conditioners Used To Compare the Ratio of Condenser Fan Power Consumption to the Power Consumption of the Compressor and the Condenser Fan**

	RTU	Split Air Conditioners
<b>Number of units</b>	60	30
<b>Number of brands</b>	6	4
<b>Range of rated cooling capacity (kW)</b>	6 to 108	5 to 73
<b>Average ratio of condenser fan power consumption to the power consumption of compressor and condenser fan</b>	0.092	0.053

The model was imposed within the SEB model, and the results are shown in Table D-14 and Table D-15.

**Table D-14. Changes in Simulation Result of SEB Model  
Because of 30% Condenser Fan Motor Efficiency Degradation as  
Estimated by the RTU Condenser Fan Motor Efficiency Degradation Model**

	<b>Changes in Electricity Consumption from Nonfaulted Case (%)</b>	<b>Changes in Gas Consumption from Nonfaulted Case (%)</b>
<b>Compressor and condenser fan of the split system</b>	+4.0	N/A
<b>Blower in the indoor air ducts</b>	+0.0	N/A
<b>Gas furnace</b>	N/A	+0.0
<b>Overall</b>	+0.3	+0.0

**Table D-15. Changes in Simulation Result of SEB Model  
Because of 30% Condenser Fan Motor Efficiency Degradation as Estimated by the  
Condenser Fan Motor Efficiency Degradation Model for Split Air Conditioners**

	<b>Changes in Electricity Consumption from Nonfaulted Case (%)</b>	<b>Changes in Gas Consumption from Nonfaulted Case (%)</b>
<b>Compressor and condenser fan of the split system</b>	+2.3	N/A
<b>Blower in the indoor air ducts</b>	+0.0	N/A
<b>Gas furnace</b>	N/A	+0.0
<b>Overall</b>	+0.2	+0.0

Table D-14 and Table D-15 show that condenser fan motor efficiency degradation does not significantly affect the energy consumption of the building. The condenser fan uses only a small portion of the cooling equipment power consumption as shown by the average ratio being smaller than 10% in Table D-13, and the fault does not affect any equipment operation other than the condenser fan power consumption. Hence the fault increases the electricity consumption of the DX unit by less than 4% and increases the electricity consumption of the building by less than 0.3%.

## Appendix E: Chiller Faults

This section describes empirical models to simulate the effects of chiller faults on buildings by adjusting the empirical chiller model in EnergyPlus. This includes the following faults.

- Overcharged chillers
- Excessive oil in chillers
- Noncondensable entrainment in refrigerant flow in chillers
- Condenser fouling in chillers.

Because only steady-state data of a 90-ton water-cooled centrifugal chiller were available to train the empirical model of fault impacts from Comstock (1999), only models that are applicable to the same type of chillers were made. The data also did not include the impact of faults on the maximum cooling capacity of the chiller. However, the chiller has continuous capacity control so the loss of maximum capacity is an issue only if it were insufficient to meet load requirements. Therefore, only empirical models of the impact of faults on chiller power consumption were made using the form shown in equation (E-1).

$$\frac{\dot{W}_{chiller,F}}{\dot{W}_{chiller}} = 1 + F^2(c_{chiller,1} + c_{chiller,2}T_{w,evap,out} + c_{chiller,3}T_{w,cond,in} + c_{chiller,4}\frac{\dot{Q}_{chiller}}{\dot{Q}_{chiller,rat}} + c_{chiller,5}(\frac{\dot{Q}_{chiller}}{\dot{Q}_{chiller,rat}})^2)^2 \quad (E-1)$$

Equation (E-1) does not change the building model when the fault level  $F$  is zero and the chiller power consumption always increases with an increase of fault level. Water outlet temperature of the evaporator and chiller cooling load are inputs in equation (E-1) because the water outlet temperature was controlled by the chiller compressor control and the cooling load is uniquely determined for a given inlet temperature and flow when the outlet temperature is specified. The applicability of equation (E-1) is governed by the range of steady-state data from Comstock (1999) as tabulated in Table E-1.

**Table E-1. Testing Conditions of Training Data of Chiller Fault Models**

Variable	Range
Water outlet temperature of the evaporator (°C)	4.0 to 11.6
Water inlet temperature of the condenser (°C)	17.8 to 30.0
Ratio of cooling capacity to the reference cooling capacity of the chiller in EnergyPlus	0.27 to 1

The model was trained by minimizing the sum of squares of the chiller power consumption between the estimated values and the training data. The range of fault levels in the testing data and the training results of the models are described in the following subsections. The definition of fault level in this section follows the ones in Comstock (1999), and they may differ from those in other sections despite their similarities.

## E.1 Overcharged Chillers

Chillers become overcharged when technicians accidentally charge more refrigerant than the manufacturer recommendation into the chiller during installation or maintenance. This increases the mass of refrigerant in the condenser, the compressor discharge pressure, and hence the compressor power consumption.

The fault level is defined as the percentage difference between the mass of refrigerant in the chiller and the recommended mass of refrigerant in the chiller according to the chiller manufacturer. The training of the model was conducted with data of fault levels of 100% to 140%. The accuracy of the model is accessed by the statistics in Table E-2.

**Table E-2. Statistics of the Accuracy of Overcharging Model for Chillers**

$r^2$	0.8468
Maximum deviation	0.03

Table E-2 shows a coefficient of determination lower than 0.9 and a maximum deviation at 0.03. The reason for the low coefficient of determination and maximum deviation is caused by the small range of fault impact ratios. Although the maximum deviation is low, the range of fault impact ratios in the training data is 1 to 1.13 only. So an insignificant deviation of 0.03 for energy input ratio becomes significant relative to the range of fault impact ratios in the training data. This results in the low coefficient of determination in Table E-2.

The fault model was used to simulate the impact of overcharging in buildings to see if it increases the energy consumption, and the results are shown in Table E-3.

**Table E-3. Changes in MEC Building Performance With Chiller Overcharged at 30%**

	Changes in Electricity Consumption from Nonfaulted Case (%)	Changes in Gas Consumption from Nonfaulted Case (%)
Chiller and cooling tower	+1.4	N/A
Blower in the indoor air ducts	+0.0	N/A
Gas boiler	N/A	+0.0
Pumps for water flow in the chiller, cooling tower, and boiler	+0.0	N/A
Overall	+1.1	+0.0

The results in Table E-3 show that the overcharged chiller increases the building's electricity consumption by 0.7%, showing that the energy consumption is increased by the fault.

## E.2 Excessive Oil in Chillers

Chillers may also get more oil than the manufacturer's recommendation during installation or maintenance. If this happens, more refrigerant will dissolve in the oil than the normal condition,

and the effective mass of refrigerant circulating in the chiller will be lower than that of the normal condition. If the chiller is running without enough refrigerant, it will work like an undercharged air conditioner and will need more power consumption to provide the same cooling capacity as normal operation.

The fault level is defined as the percentage difference between the oil in the chiller and the recommended mass of oil from the chiller manufacturer, and the range of the fault level in the training data is between 0% and 73%. The estimation results are illustrated in Table E-4.

**Table E-4. Statistics of the Accuracy of Excessive Oil Model for Chillers**

$r^2$	0.7709
<b>Maximum deviation</b>	0.03

The coefficient of determination and the maximum deviation in Table E-4 are low for similar reasons as the overcharging model in Table E-2. The range of fault impact ratios of chiller power consumption in the training data is between 0.98 and 1.07 only. Although the maximum deviation is acceptable for the estimation of power consumption, it is significant relative to the range of fault impact ratios in the training data. This causes the low coefficient of determination despite the acceptable maximum deviation value.

To verify the fault model, it was used to simulate the impact of excessive oil in chillers to the building energy consumption of the MEC. The results are shown in Table E-5.

**Table E-5. Changes in MEC Building Performance with the Chiller Faulted by Excessive Oil at 70%**

	<b>Changes in Electricity Consumption from Nonfaulted Case (%)</b>	<b>Changes in Gas Consumption from Nonfaulted Case (%)</b>
<b>Chiller and cooling tower</b>	+4.9	N/A
<b>Blower in the indoor air ducts</b>	+0.0	N/A
<b>Gas boiler</b>	N/A	+0.0
<b>Pumps for water flow in the chiller, cooling tower, and boiler</b>	+0.0	N/A
<b>Overall</b>	+3.7	+0.0

Table E-5 shows that energy consumption of the building is increased by the additional oil in the chiller.

### **E.3 Noncondensable Entrainment in Refrigerant in Chillers**

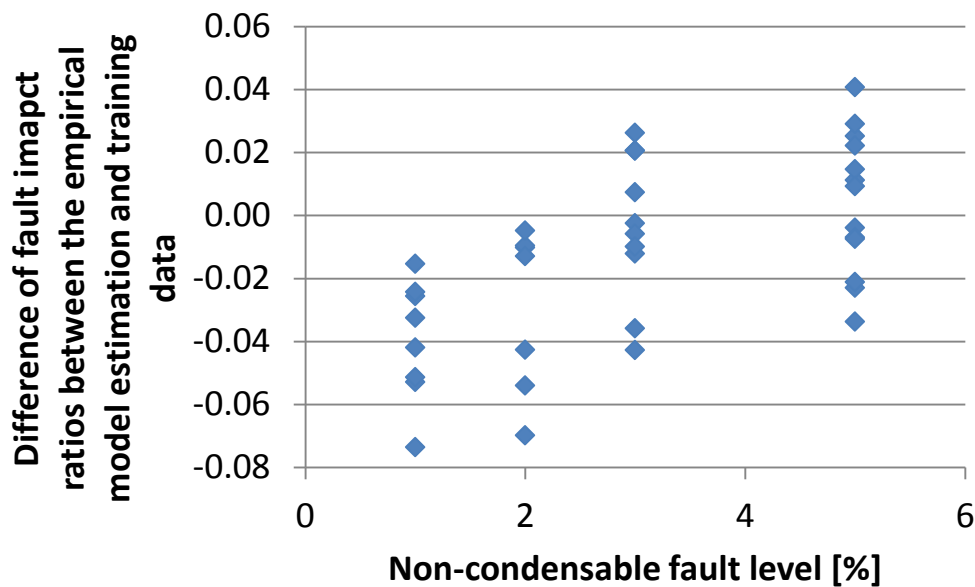
Similar to air conditioners, air can enter chillers if the refrigerant circuit is not properly evacuated before the refrigerant is charged. The noncondensable entrainment affects the refrigerant circuit of a chiller the same way as it does an air conditioner: it increases compressor power consumption.

The fault level is defined as the ratio of the volume of the noncondensable in the chiller to the volume of the noncondensable in the chiller at atmospheric pressure and temperature. The range of the fault level in the training data is 0% to 5%. The estimation results are illustrated in Table E-6.

**Table E-6. Statistics of the Accuracy of Noncondensable Entrainment Fault Model for Chillers**

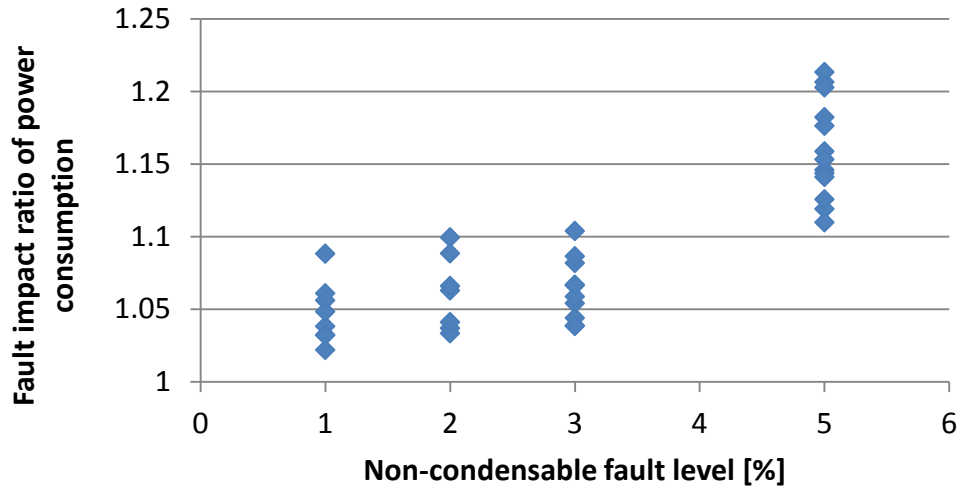
$r^2$	0.6852
Maximum deviation	0.07

Table E-6 shows a low coefficient of determination and a high maximum deviation. To examine the cause, the deviation of the estimation with the training data is plotted in Figure E-1.



**Figure E-1. Change of estimation deviation of the chiller noncondensable entrainment fault model with the fault level**

To examine why the maximum deviation occurs at low fault level, the change of training data fault impact ratio with the fault level is plotted in Figure E-2.



**Figure E-2. Change of fault impact ratio of power consumption with noncondensable entrainment fault level**

Figure E-2 shows that the fault impact ratios of power consumption for fault levels of 1% to 3% are almost identical. Because it is difficult to find a mathematical expression to model the change, the model is left as is despite its relatively low accuracy compared to other models.

To examine if the fault model can predict the increase of building energy consumption, it was used to simulate the impact of noncondensable entrainment in chillers to the building energy consumption of the MEC. The results are shown in Table E-7.

**Table E-7. Changes in MEC Building Performance with the Chiller Faulted by Noncondensable Entrainment in Refrigerant at 5%**

	Changes in Electricity Consumption from Nonfaulted Case (%)	Changes in Gas Consumption from Nonfaulted Case (%)
Chiller and cooling tower	+11.5	N/A
Blower in the indoor air ducts	+0.0	N/A
Gas boiler	N/A	+0.0
Pumps for water flow in the chiller, cooling tower, and boiler	+0.0	N/A
Overall	+8.7	+0.0

Table E-7 shows that the building’s energy consumption is increased by the noncondensable. Despite the low accuracy of the empirical model, the noncondensable entrainment model can predict an increase of electricity consumption with the fault level.

## E.4 Condenser Fouling in Chillers

Condensers chillers are fouled by sediment that blocks the water flow paths in the chiller condenser. When the condenser is fouled, the water flow cannot reach all the heat transfer surfaces inside the condenser. This increases the condensing pressure and the pressure difference across the compressor and hence leads to higher condenser power consumption.

The fault level definition of condenser fouling is the percentage of water flow paths blocked in the condenser. The fault levels in the training data range from 0% to 45%. The accuracy of the empirical model trained is shown in Table E-8.

**Table E-8. Statistics of the Accuracy of Condenser Fouling Model for Chillers**

$r^2$	0.7312
<b>Maximum deviation</b>	0.03

The accuracy of the empirical model in Table E-8 is similar to that of the excessive oil model in Table E-4 where the low coefficient of determination is caused by the small range of fault impact ratios in the training data. For this fault, the training data fault impact ratio of chiller power consumption ranges from 1 to 1.10, which is similar to that of the training data of the excessive oil fault empirical model. The coefficient of determination calculation compares the deviation between the model estimates and the training data with the range of fault impact ratios instead of the required accuracy, leading to an impression that the model is not accurate enough for application.

The condenser fouling model verification was done by the simulation of the impact of chiller condenser fouling to the MEC. The simulation results are shown in Table E-9.

**Table E-9. Changes in MEC Building Performance with the Chiller Faulted by Condenser Fouling at 40%**

	<b>Changes in Electricity Consumption from Nonfaulted Case (%)</b>	<b>Changes in Gas Consumption from Nonfaulted Case (%)</b>
<b>Chiller and cooling tower</b>	+3.0	N/A
<b>Blower in the indoor air ducts</b>	+0.0	N/A
<b>Gas boiler</b>	N/A	+0.0
<b>Pumps for water flow in the chiller, cooling tower, and boiler</b>	+0.0	N/A
<b>Overall</b>	+2.3	+0.0

The results in Table E-9 show that the model predicts an electricity consumption increase of the chiller by condenser fouling.

## Appendix F: Other Uncategorized Faults

The detailed modeling approaches of other faults that are not categorized in this report are described in this section of the appendix. They include the following faults.

- Duct fouling
- Fan and pump motor efficiency degradation
- Excessive infiltration around building envelope.

Similar to the other sensor and control faults, the fault models in this group were verified by imposing them within the MEC model to see if the prediction is reasonable. If the fault model was applicable to more than one device, the fault model was imposed within all of them at the same fault level.

### F.1 Duct Fouling

Ducts are fouled by dust that accumulates in the filter and/or fins of heat exchangers in the indoor air ducts. The accumulation increases the flow resistance of the air duct and changes the airflow and pressure drop across the duct in accordance with the controls of the fan rotational speed. To illustrate the changes of fan and duct operation by duct fouling, fan and duct curves are drawn as shown in Figure F-1.

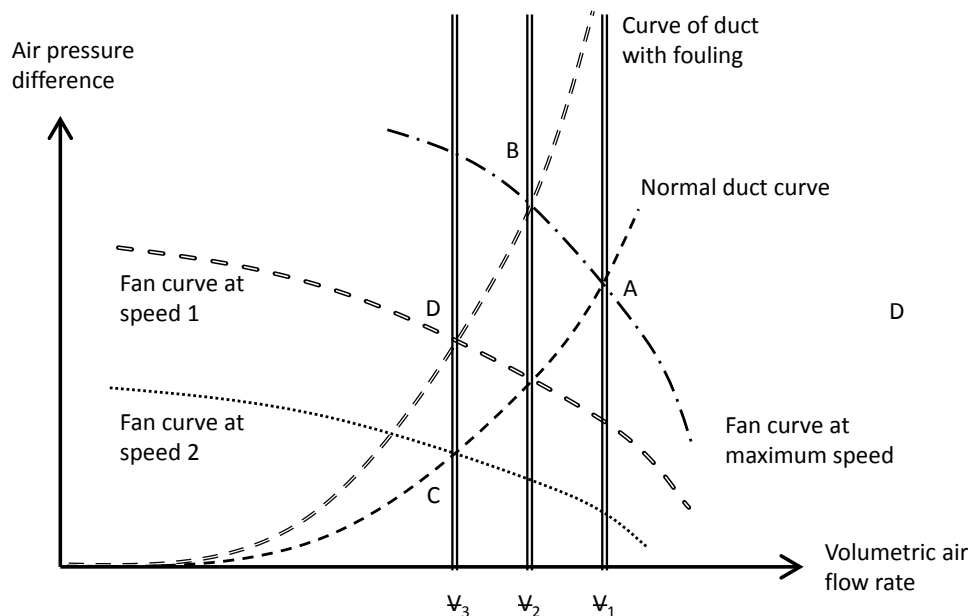


**Figure F-1. Fan and duct curves under normal and fouling condition**

For single-speed blowers, the operating point of the blowers can be found at A in Figure F-1 in a nonfaulted condition. When the duct is fouled, the duct curve shifts upward, and the fan

operating point shifts from A to B. The pressure difference across the duct increases, and the airflow drops.

For variable-speed blowers with identical maximum speed, the nonfaulted operating point of the fans can usually be found on a fan curve at a lower speed such as C in Figure F-1. When the duct is fouled, the blower increases from speed 2 to speed 1 to maintain a constant airflow at  $\Psi_3$ . Hence the airflow remains constant and the pressure difference increases.

The fault level is defined by the percentage increase of the pressure difference along the fan curve at the maximum speed due to duct fouling to represent the increase of its flow resistance. For instance, if the duct is fouled and the duct curves shift from the normal curve to the fouled curve in Figure F-1, the fault level is defined by the percentage increase of pressure difference from point A to B in Figure F-1, including ducts with variable-speed fans.

The change of airflow along the maximum speed fan curve in Figure F-1 is needed to model the duct fouling impact in ducts with single-speed blowers. However, the EnergyPlus single-speed fan models (Fan:ConstantVolume and Fan:OnOff) do not contain any fan curves. Hence a semiempirical and normalized fan curve is needed in the duct fouling model to simulate the changes of airflow and pressure difference by duct fouling as shown in Figure F-1. The fan curve is provided by simplifying the ideal centrifugal fan model from Osborne (1977) as equation (F-1).

$$\frac{\Delta P_{fan}}{\Delta P_{fan,rat}} = c_{fan,0} \left( \frac{freq}{freq_{rat}} \right)^2 + c_{fan,1} \left( \frac{freq}{freq_{rat}} \right) \left( \frac{\Psi}{\Psi_{rat}} \right)^2 \quad (F-1)$$

By having the normalized terms in equation to be equal to one at nonfaulted conditions, an equation with one coefficient only can be formed from equation (F-1). The resultant duct fouling model is equation (F-2).

$$\frac{\Delta P_{fan}}{\Delta P_{fan,rat}} = c_{fan,0} \left( \frac{freq}{freq_{rat}} \right)^2 + (1 - c_{fan,0}) \left( \frac{freq}{freq_{rat}} \right) \left( \frac{\Psi}{\Psi_{rat}} \right)^2 \quad (F-2)$$

Because EnergyPlus needs an air mass flow rate instead of air volumetric flow rate, air mass flow rate ratio is used to replace the air volumetric flow rate ratio in equation (F-2). For single-speed fans, the rotational speed ratio in equation (F-2) can be set to 1. The denominators of the normalized terms in equation (F-2) are adjusted to give one at the nonfaulted condition. This gives the duct fouling model of single-speed fan that changes the pressure difference and the air mass flow rate as equations (F-3) and (F-4).

$$\Delta P_{fan,F} = \Delta P_{fan,rat} (1 + F) \quad (F-3)$$

$$\dot{m}_{a,fan,F} = \dot{m}_{a,rat} \sqrt{\frac{1 + F - c_{fan,0}}{1 - c_{fan,0}}} \quad (F-4)$$

For variable-speed fans, EnergyPlus uses a normalized empirical model in Fan:VariableVolume model to compute the fan power consumption at different rotational speeds along the duct curve

in Figure F-1. Because adjusting the empirical equation that computes the intermediate speed condition is difficult, assuming that the normalized empirical equation is not changed by duct fouling, equations (F-3) and (F-4) are used to adjust the operating condition of the blower at maximum speed to simulate the duct fouling impact on the building model. This implies that the empirical equation will use airflow and pressure difference at point B instead of point A in Figure F-1 to compute its power consumption at point D when the duct is fouled. Because calculating the effect of fouling on the minimum blower power consumption is difficult, the magnitude of the minimum fan power consumption of the variable-speed fan is set to remain unchanged before and after fouling.

To estimate the coefficient in equation (F-4), pressure differences, rotational speeds, and volumetric airflow rates were collected from the specification of blowers in three RTUs. They were normalized relative to the highest speed and pressure difference data available in their data set, assuming that the data point is the most probable operating point at the rated condition. The three data sets were used separately to find three different equations (F-4) by linear regression, and their coefficients were averaged to obtain the final coefficient  $c_{fan,0}$ . The resultant model accuracy is shown in Table F-1.

**Table F-1. Statistics of the Accuracy of Condenser Fouling Model for Chillers**

$r^2$	0.9291
Maximum deviation	0.17

The large maximum deviation in Table F-1 is studied by examining the residual plot Figure F-2.

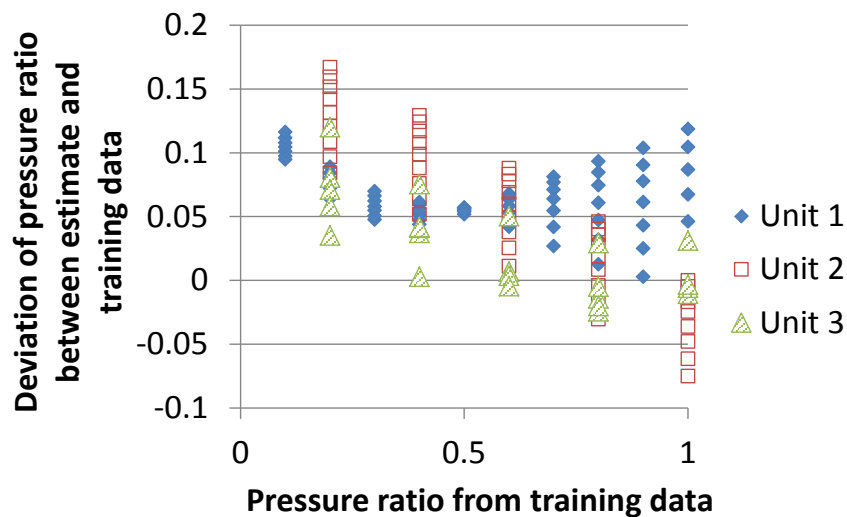


**Figure F-2. Residual plot of estimated pressure difference ratio across fans**

Figure F-2 shows that the maximum deviation occurs when the pressure difference ratio is 0.2. As equation (F-4) is used only to adjust the maximum speed operating point, it seldom alters the operation with a pressure ratio across the blower to be 20% of its maximum value and the accuracy of the model is acceptable.

To verify the fault model, the fault model was used with the MEC model to determine if its estimated impact is reasonable. Because the MEC model has variable-speed fan models, the fan energy consumption is expected to increase. The simulation results are shown in Table F-2.

**Table F-2. Changes in MEC Building Performance by Duct Fouling at 10%**

	<b>Changes in Electricity Consumption from Nonfaulted Case (%)</b>	<b>Changes in Gas Consumption from Nonfaulted Case (%)</b>
<b>Chiller and cooling tower</b>	+0.1	N/A
<b>Blower in the indoor air ducts</b>	+12.2	N/A
<b>Gas boiler</b>	N/A	-0.1
<b>Pumps for water flow in the chiller, cooling tower, and boiler</b>	+0.0	N/A
<b>Overall</b>	+0.4	-0.1

Table F-2 shows that duct fouling increases the electricity consumption of the blower. In this building model, the AHU blowers usually ran with intermediate rotational speed. When the AHUs were subjected to duct fouling, the power consumption of the blowers changed from operating point C to operating point D as shown in Figure F-1. Hence duct fouling increased the blower energy consumption in this case.

## F.2 Blower and Pump Motor Efficiency Degradation

Blower and pump motor efficiency degrades mainly because of bearing and stator winding faults, as discussed in the previous subsections on condenser fan motor efficiency degradation. Their fault levels can be defined the same way as the percentage reduction of motor efficiency, and the fault model in equation (D-15) can be used to simulate the impact of these faults.

To determine whether the fault models increase the blower and pump power consumption in a building simulation program, they were used with the MEC model. The results are tabulated in Table F-3 and Table F-4.

**Table F-3. Changes in MEC Building Performance by Blower Motor Efficiency Degradation at 25%**

	<b>Changes in Electricity Consumption from Nonfaulted Case (%)</b>	<b>Changes in Gas Consumption from Nonfaulted Case (%)</b>
<b>Chiller and cooling tower</b>	+0.4	N/A
<b>Blower in the indoor air ducts</b>	+33.2	N/A
<b>Gas boiler</b>	N/A	-0.3
<b>Pumps for water flow in the chiller, cooling tower, and boiler</b>	+0.0	N/A
<b>Overall</b>	+1.2	-0.4

**Table F-4. Changes in MEC Building Performance by Pump Motor Efficiency Degradation at 15%**

	<b>Changes in Electricity Consumption from Nonfaulted Case (%)</b>	<b>Changes in Gas Consumption from Nonfaulted Case (%)</b>
<b>Chiller and cooling tower</b>	+0.2	N/A
<b>Blower in the indoor air ducts</b>	+0.0	N/A
<b>Gas boiler</b>	N/A	-0.3
<b>Pumps for water flow in the chiller, cooling tower, and boiler</b>	+17.7	N/A
<b>Overall</b>	+1.1	-0.3

Table F-3 shows that the blower power consumption is increased by the fault model. The increased fan power consumption increases the fan heat, and the chiller compensates for the fan heat by consuming more electricity to provide more cooling. At the same time, the fan heat reduces the amount of gas needed to keep the building warm in heating season, and the gas consumption is reduced.

Table F-4 shows that the pump motor efficiency degradation increases the pump power consumption. Part of the pump power consumption is transferred to the water stream and heats the water entering the AHUs. To maintain the temperature of the water coils in the AHUs at the set point, the chiller and cooling tower consume more electricity to cool down the water, and the boiler consumes less gas to reduce the water temperature in heating operation.

### **F.3 Excessive Infiltration around Building Envelope**

Excessive infiltration around the building envelope occurs when building occupants accidentally leave windows and doors open and let air enter the building through these unnecessary openings. The fault level is defined as the percentage increase of infiltration airflow rate compared to the nonfaulted case. The excessive infiltration permits extra hot air to enter the indoors during cooling season and extra cold air to enter indoors during heating season, increasing the demand for space conditioning on the building equipment and increasing the energy consumption for space conditioning.

To examine whether the fault model increases energy consumption from space conditioning equipment, the fault model was used to simulate the impact of excessive infiltration on the MEC. The results are shown in Table F-5.

Results in Table F-5 show that the fault model increases the energy consumption of the chiller, the cooling tower and the boiler. It also increases the energy consumption of the blower because it lengthens its operation time to meet the increased demand for space conditioning.

**Table F-5. Changes in MEC Building Performance by Excessive Infiltration at 30%**

	<b>Changes in Electricity Consumption from Nonfaulted Case (%)</b>	<b>Changes in Gas Consumption from Nonfaulted Case (%)</b>
<b>Chiller and cooling tower</b>	+0.6	N/A
<b>Blower in the indoor air ducts</b>	+10.4	N/A
<b>Gas boiler</b>	N/A	+13.3
<b>Pumps for water flow in the chiller, cooling tower, and boiler</b>	-0.5	N/A
<b>Overall</b>	+0.7	+13.3